Miner Deposita (2007) 42:715–735
DOI 10.1007/s00126-007-0135-5

ARTICLE

The New Consort Gold Mine, Barberton greenstone belt, South Africa: orogenic gold mineralization in a condensed metamorphic profile

A. Otto · A. Dziggel · A. F. M. Kisters · F. M. Meyer

Received: 14 December 2006 / Accepted: 14 March 2007 / Published online: 3 April 2007

Abstract The New Consort Gold Mine in the Palaeo- to Mesoarchaean Barberton greenstone belt, South Africa is one of the oldest recognized orogenic gold deposits on Earth. The gold mineralization is hosted by discrete mylonitic units that occur at, or close to, the contact between the mafic and ultramafic volcanic rocks of the c. 3,280 Ma Onverwacht Group and the mainly metasedimentary rocks of the overlying c. 3,260–3,230 Ma Fig Tree Group. This contact, locally referred to as the Consort Bar, formed during ductile D_1 imbrication of the metavolcano-sedimentary sequence and predates the main stage of the gold mineralization. The imbricate stack is situated in the immediate hanging wall of the basal granitoid–greenstone contact along the northern margin of the greenstone belt. It is characterized by a condensed metamorphic profile in which the metamorphic grade increases from upper greenschist facies conditions (510–530°C, 4 kbar) in rocks of the Fig Tree Group to upper amphibolite facies grades (600–700°C, 6–8 kbar) in the basal Onverwacht Group. Detailed structural and petrological investigations indicate that the Consort Bar represents a major structural break, which is largely responsible for the telescoping of metamorphic isograds within the structural sequence. Two stages of mineralization can be distinguished. Loellingite, pyrrhotite, and a calc–silicate alteration assemblage characterize an early high-T mineralization event, which is restricted to upper amphibolite facies rocks of the Onverwacht Group. This early mineralization may correlate with the local D_1 deformation. The second and main stage of gold mineralization was associated with renewed ductile shearing during D_2. The D_2 deformation resulted in the reactivation of earlier structures, and the formation of a NNW trending, steeply dipping shear zone system, the Shires Shear Zone, which separates two regional SE plunging D_1 synclines. The mineralized shear zones are intruded by abundant syn-kinematic pegmatite dykes that have previously been dated at c. 3040 Ma. Petrological and geothermobarometric data on ore and alteration assemblages indicate that the main stage of gold mineralization, which affected a crustal profile of ca. 1.5 km, was characterized by increasing temperatures (c. 520 to 600°C) with increasing structural depth. Sulfide assemblages in the ore bodies change progressively with metamorphic grade, ranging from arsenopyrite + pyrite + pyrrhotite in the structurally highest to arsenopyrite + pyrrhotite + chalcopyrite + loellingite in the structurally deepest part of the mine. The main stage of gold mineralization was broadly syn-peak metamorphic with respect to the Fig Tree Group, but postdates the peak of metamorphism in upper amphibolite facies rocks of the structurally underlying Onverwacht Group. This indicates that the mineralization coincided with the juxtaposition of the two units. As the footwall rocks were already on their retrograde path, metamorphic devolatilisation reactions within the greenstone sequence can be ruled out as the source of the mineralizing fluids.

Keywords Orogenic gold · Barberton greenstone belt · South Africa · New Consort

Editorial handling: H. Frimmel

A. Otto (✉) · A. Dziggel · F. M. Meyer
Institute of Mineralogy and Economic Geology,
RWTH Aachen University,
Wuellnerstr. 2,
52062 Aachen, Germany
e-mail: otto@iml.rwth-aachen.de

A. F. M. Kisters
Department of Geology, University of Stellenbosch,
Private Bag X1, Matieland,
7602 Stellenbosch, South Africa

Introduction

Structurally controlled orogenic gold deposits form as an integral part of subduction-related accretionary or collisional orogenies, typically during the late stages of the tectono-metamorphic evolution of the respective terranes (e.g., Kerrich and Cassidy 1994; Groves et al. 1998, 2000, 2003; Witt and Vanderhor 1998; McCuaig and Kerrich 1998; Hagemann and Cassidy 2000; Goldfarb et al. 2005). These deposits are characterized by high gold to base metal ratios, relative low sulfide content, a variable addition of K, As, Sb, LILE, CO_2, and S to the deformed wall rocks, and low-salinity H_2O–CO_2(–CH_4) ore fluids. Although most of these deposits formed under greenschist facies conditions, the P–T conditions of formation have been documented to extend from sub-greenschist to upper amphibolite or even granulite facies conditions, equivalent to crustal depths ranging between c. 5 and 20 km (Groves 1993; Groves et al. 2003). To date, only a few gold camps have been identified in which a transition in metamorphic grade coupled with a distinct change in the style of alteration and mineralization can be recorded (e.g., Red Lake, Superior province: Andrews et al. 1986; Norseman goldfields: McCuaig et al. 1993). The Palaeo- to Mesoarchaean Barberton greenstone belt in South Africa (Fig. 1) hosts some of the oldest recognized orogenic gold deposits on Earth (Goldfarb et al. 2001). The majority of gold deposits in the greenstone belt occur along the southern contact of the c. 3,227±1 Ma Kaap Valley pluton (Kamo and Davis 1994; Fig. 1) and are hosted by greenschist facies supracrustal rocks (Schouwstra and deVilliers 1988; de Ronde et al. 1992; Robertson et al. 1994; Schouwstra 1995; Schürmann et al. 2000). Based on fluid inclusion data and sulfide geothermobarometry, the P–T condition of mineralization have been estimated at c. 300 to 425°C and 1 to 4 kbar (de Ronde et al. 1992; Schouwstra and deVilliers 1988). In contrast to these greenschist facies deposits, the gold mineralization at the New Consort Gold Mine is situated within rocks of distinctly higher metamorphic grade, close to the granitoid–greenstone contacts along the northern margin of the belt (Fig. 1). Currently available temperature estimates of 520 to 580°C indicate amphibolite facies conditions of metamorphism and mineralization (Tomkinson and Lombard 1990). A unique feature of the gold mineralization at New Consort is the development of relatively continuous and laterally extensive mineralized horizons in wall rocks of significantly different metamorphic grade. This offers the opportunity to study the controls and timing of a hydrothermal plumbing system under different metamorphic and rheologic conditions in one mine. To establish the relative timing of gold mineralization with respect to the structural and metamorphic evolution of

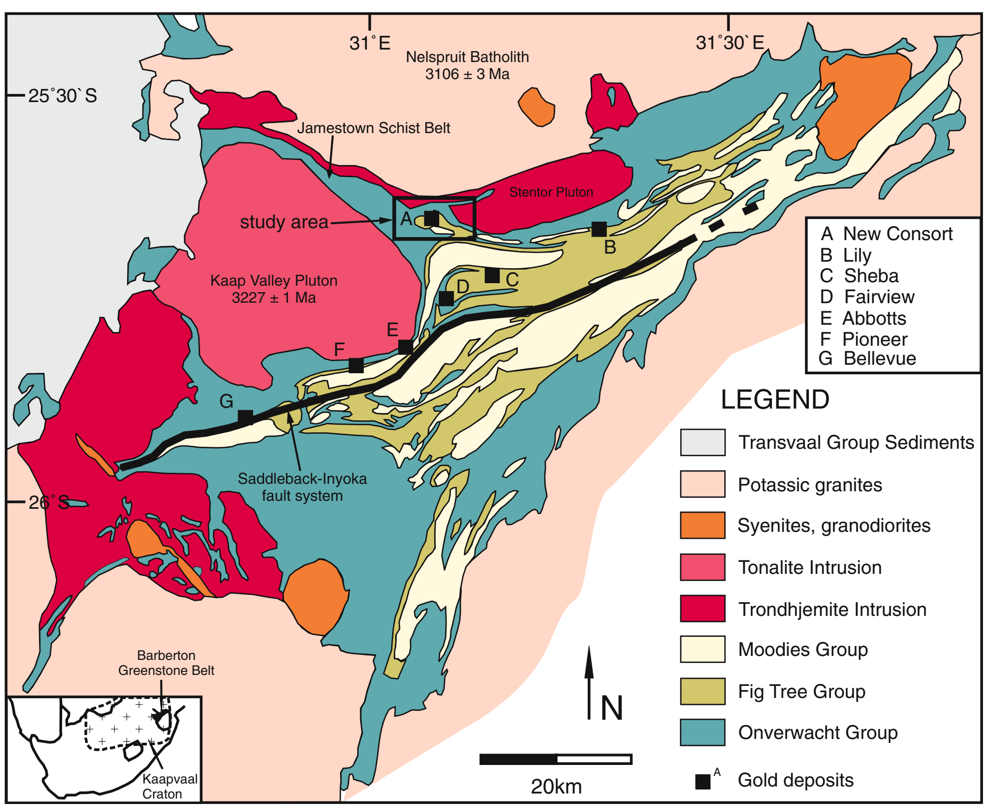

Fig. 1 Generalized geological map of the Barberton greenstone belt, South Africa modified after de Ronde and de Wit (1994). Geochronological data are from Kamo and Davis (1994). The *bold line* represents the Saddleback–Inyoka Fault System

the wall rocks, we have studied three selected localities that are located, from west to east, in progressively higher-metamorphic wall rocks. In the following, the three localities will be referred to as the Western, Central, and Eastern Zones. We will first characterize the different P–T conditions of the regional metamorphism experienced by the wall rocks and then describe the petrologic variations of ore- and alteration parageneses between the different localities.

Regional geology

The Barberton greenstone belt is situated in the eastern part of the Mpumalanga Province, South Africa (Fig. 1). Metamorphism is generally low-grade but increases towards the margins of the belt to upper amphibolite facies conditions (Cloete 1999; Dziggel et al. 2002, 2006; Diener et al. 2005). The c. 3550–3230 Ma greenstone sequence forms the Swaziland Supergroup and has been subdivided into three major lithostratigraphic units, including the basal, predominantly metavolcanic Onverwacht Group, and the overlying sedimentary Fig Tree and Moodies Groups (SACS 1980). A major suture zone in the central parts of the belt, termed the Saddleback–Inyoka Fault System, separates a northern from a southern terrane in the belt (de Ronde and de Wit 1994). Onverwacht Group rocks of the southern terrane range in age between c. 3550 and 3300 Ma (Kröner et al. 1996; Byerly et al. 1996), whereas Onverwacht Group rocks of the northern terrane, which host all of the major gold deposits, have been dated at 3,286±29 Ma (Lahaye et al. 1995). The deposition of the Fig Tree and Moodies Groups in both terranes has been bracketed between c. 3260 and 3216 Ma (Kröner et al. 1991; Kamo and Davis 1994; Lowe and Byerly 1999). The northern terrane has been affected by two major tectono-magmatic events. The earlier event represents the main collision of the northern and southern terranes of the Barberton greenstone belt, which has been bracketed between 3,229 and 3,227 Ma (de Ronde and Kamo 2000). This event was accompanied by TTG (tonalite–trondhjemite–granodiorite) magmatism, as exemplified by the 3,227±1 Ma Kaap Valley Tonalite (Kamo and Davis 1994; Fig. 1). The second event is characterized by the emplacement of sheet-like potassic granites, including the 3,106±3 Ma Nelspruit Batholith (de Ronde and de Wit 1994; Kamo and Davis 1994; Fig. 1). It has been suggested that this late-tectonic history was associated with a change from convergent to transtensional (extensional) tectonics (de Ronde and de Wit 1994). The shear-zone-hosted gold mineralization has been proposed to

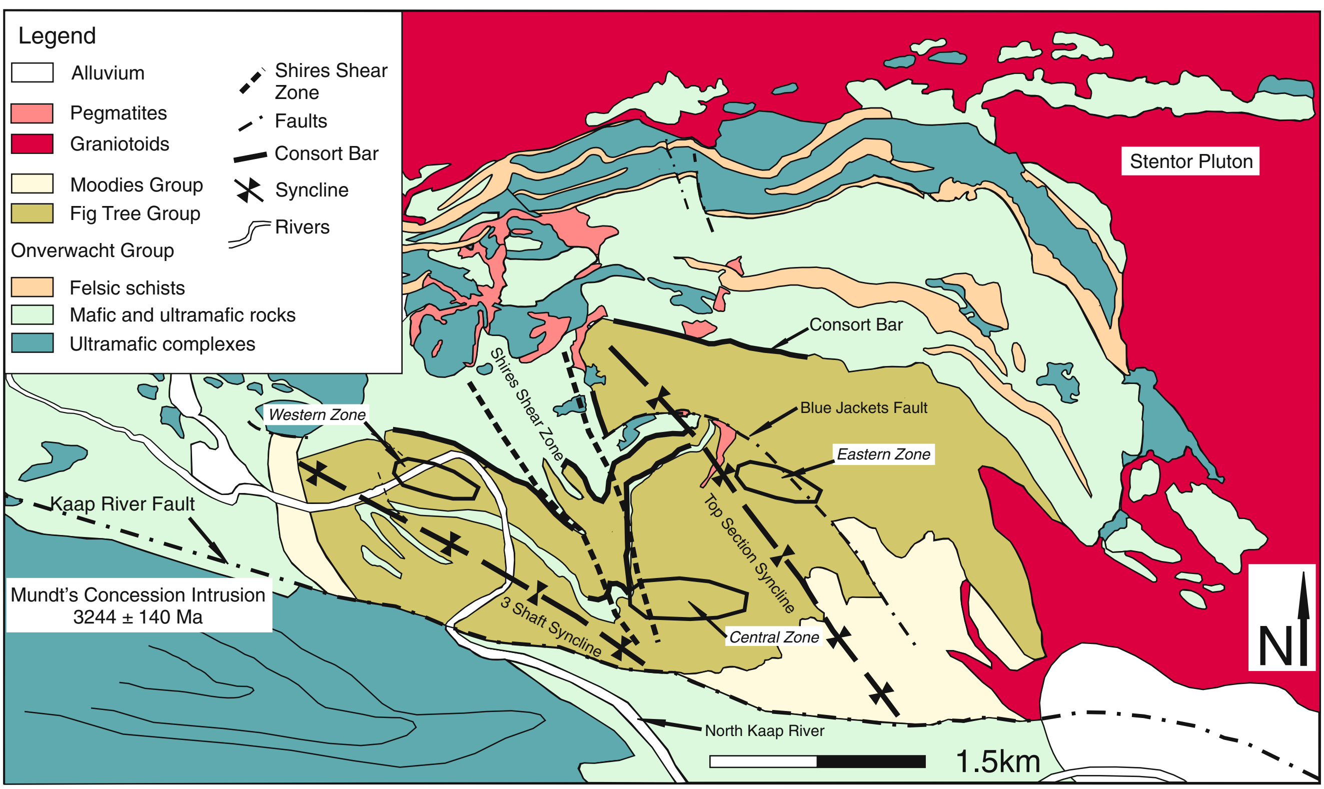

Fig. 2 Simplified geological map of the New Consort Gold Mine area in the eastern part of the Jamestown schist belt (modified after Anhaeusser and Viljoen 1965; Anhaeusser 1972). The investigated areas, namely the Western, Central, and Eastern Zones are projected from underground and correspond to a depth of c. 150 m, c. 1,400 m, and c. 1,400 m, respectively. The age for the Mundt's Concession Intrusion is from Dupré and Arndt (1990)

correlate with this event (de Ronde et al. 1991). Time constraints are given by a c. 3,126 Ma porphyry dike predating the shearing and a c. 3,084 Ma age for hydrothermal rutile associated with the gold mineralization at Fairview Mine (de Ronde et al. 1991).

Mine geology

Since the beginning of gold production in 1884, the New Consort Gold Mine has produced more than 2.1 million ounces of Au (Anhaeusser 1986; Roelf le Roux, 2005, personal communication). The mine workings are located in the immediate hanging wall of the basal granitoid–greenstone contact in the eastern part of the Jamestown schist belt (Figs. 1 and 2). Gold mineralization is mainly structurally controlled and is closely associated with the so-called Consort Bar, a relatively thin (average thickness c. 4 m), highly silicified mylonitic shear zone that separates amphibolites and ultramafic schists of the Onverwacht Group from the overlying metapelites and metapsammites of the Fig Tree Group (Fig. 2; Anhaeusser 1986; Voges 1986). The volcano-sedimentary sequence is floored to the north and east by mid-crustal gneisses of the composite Stentor Pluton. Currently available U–Pb zircon data underline the polyphase emplacement history of the pluton, with ages of 3,347+67/−60 Ma, 3,250±30 Ma and 3,107±5 Ma for the variably deformed gneisses (Tegtmeyer and Kröner 1987; Kamo and Davis 1994). The overlying supracrustal sequence has been folded into two major synclines, namely the 3-Shaft and Top Section Synclines, with fold axes plunging at moderate to steep angles to the southeast (Anhaeusser and Viljoen 1965; Anhaeusser 1972; Harris et al. 1995). In the south, the two synclines are truncated by a late, greenschist facies shear zone, the Kaap River Fault. In the mine area, three deformation events can be distinguished. It should be noted that the sequence of deformation events refers to the local structural evolution and does not correspond to any regional tectonic event. The earliest deformation event (D_1) is characterized by the development of a pervasive, moderately south dipping S_1-foliation along the granite–greenstone contact. D_1 shearing has been interpreted as a result of extensional unroofing and doming of basement gneisses in response to the orogenic collapse of the Barberton greenstone belt during or shortly after the main accretionary episode at c. 3,230 Ma (Dziggel et al. 2006). The formation of the Consort Bar and the shallowly plunging Top Section and 3-Shaft Synclines has been correlated with this early deformation event (Tomkinson and Lombard 1990; Harris et al. 1995). The gold mineralization has been proposed to correlate with the local D_2 deformation (Harris et al. 1995) and the development of the steeply dipping Shires Shear Zone (SSZ) in the central parts of the mine (Fig. 2; Anhaeusser 1972). This up to 350 m wide shear zone system consists of an anastomosing network of subvertical shear zones, which strike N–S to NW–SE (Tomkinson and Lombard 1990; Harris et al. 1995). The shear zones are intruded by syn-kinematic (D_2) pegmatite dikes, which have been dated at c. 3,040 Ma (Harris et al. 1993, 1995). The last deformation event (D_3) is characterized by the development of brittle normal faults, collectively referred to as the Blue Jackets fault system, which crosscut all earlier structures (Fig. 2; Tomkinson and Lombard 1990; Harris et al. 1995).

Two major styles of gold mineralization have been described that are locally referred to as the Consort Contact, and Footwall Lens mineralization (Tomkinson and Lombard 1990). The Consort Contact mineralization is located within, as well as immediately (c. 2 m) below, the Consort Bar (Voges 1986). The associated auriferous sulfide-rich ore-bodies are dominated by arsenopyrite, with smaller amounts of pyrrhotite. The Footwall Lens mineralization is contained within a competent gneiss body that occurs within Onverwacht Group amphibolites below the Consort Bar (Voges 1986; Fig. 3). This type of mineralization is characterized by abundant arsenopyrite, loellingite (locally up to 70% of the ore assemblage), pyrrhotite, and chalcopyrite (Tomkinson and Lombard 1990). The size and orientation of individual ore bodies from both styles of mineralization vary depending on their exact structural position within the mine. The location of the three ore bodies investigated in this study is shown in Fig. 2. The Western Zone ore body is located on the northeastern limb

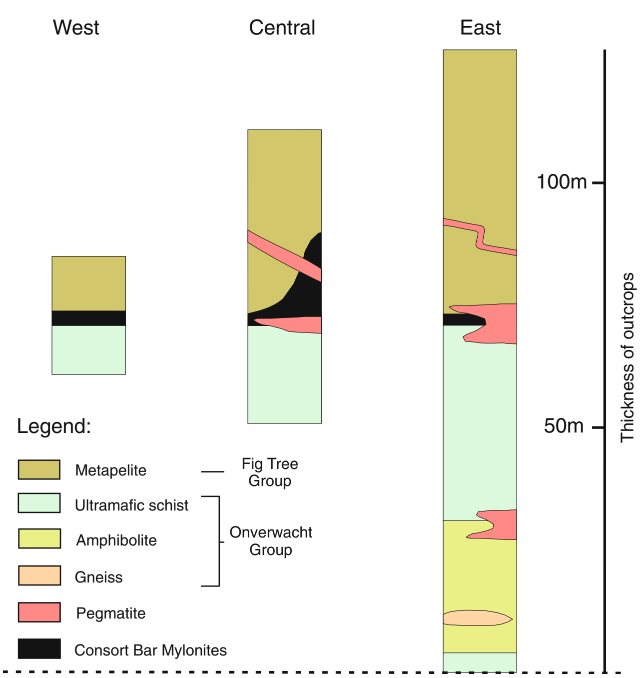

Fig. 3 Simplified stratigraphic columns showing the main lithological units in the Western, Central, and Eastern Zones

of the 3-Shaft Syncline, about 150 m below surface. The mineralization of the Central Zone is located in the Consort Bar in proximity to the Shires Shear Zone system, c. 1,400 m below surface. The Eastern Zone ore body is located c. 1,400 m below surface and c. 60 m in the footwall of the Consort Bar within the Onverwacht Group and represents an example of the Footwall Lens mineralization.

Structural development

Detailed structural mapping of the three ore bodies was carried out to establish the relative timing of deformation, metamorphism, mineralization, and magmatism. The local stratigraphy for each locality is shown in Fig. 3, and the sketches in Fig. 4 illustrate their structural evolution. After the sequence of deformation events described above, three deformation events are distinguished: (1) a D_1 deformation comprising the development of the regional S_1 foliation and subsequent regional folding; (2) a D_2 deformation characterized by renewed ductile shearing and the main stage of gold mineralization; and (3) a D_3 deformation characterized by the formation of late brittle normal faults. Deformation along the D_2 mineralized structures is commonly associated with the development of a pervasive, often mylonitic S_2 foliation that may extend for up to 5 m into the surrounding wall rocks. In the vicinity of the D_2 ore bodies, the S_2 foliation is commonly parallel to the more regionally developed S_1 (Fig. 4), either as a result of the rotation of S_1 into S_2 or because of their low-angle to parallel orientation on a regional scale. In these cases, S_1 and S_2 cannot be distinguished unequivocally so that the S_1 foliation is taken as the foliation away from the ore shoots that is exclusively defined by peak metamorphic minerals, whereas the S_2 foliation is the foliation defined by ore and alteration assemblages in proximity to, or within, the ore bodies.

In the Western Zone (Fig. 4a), the D_1 deformation is characterized by a pervasive, bedding-parallel S_1 foliation. S_1 dips at shallow angles to the SSW and is defined by peak metamorphic biotite in mylonitic metapelites and tremolite in ultramafic schists. Mineral lineations have not been observed. The thickness of the Consort Bar varies between 1 and 3 m. Ultramafic schists dominate the footwall, although drill core exposes intercalations of massive amphibolites several meters below the Consort Bar. The D_2 deformation can be subdivided into an early (D_{2a}) and a late (D_{2b}) event. The S_{2a} foliation is parallel to S_1 and is

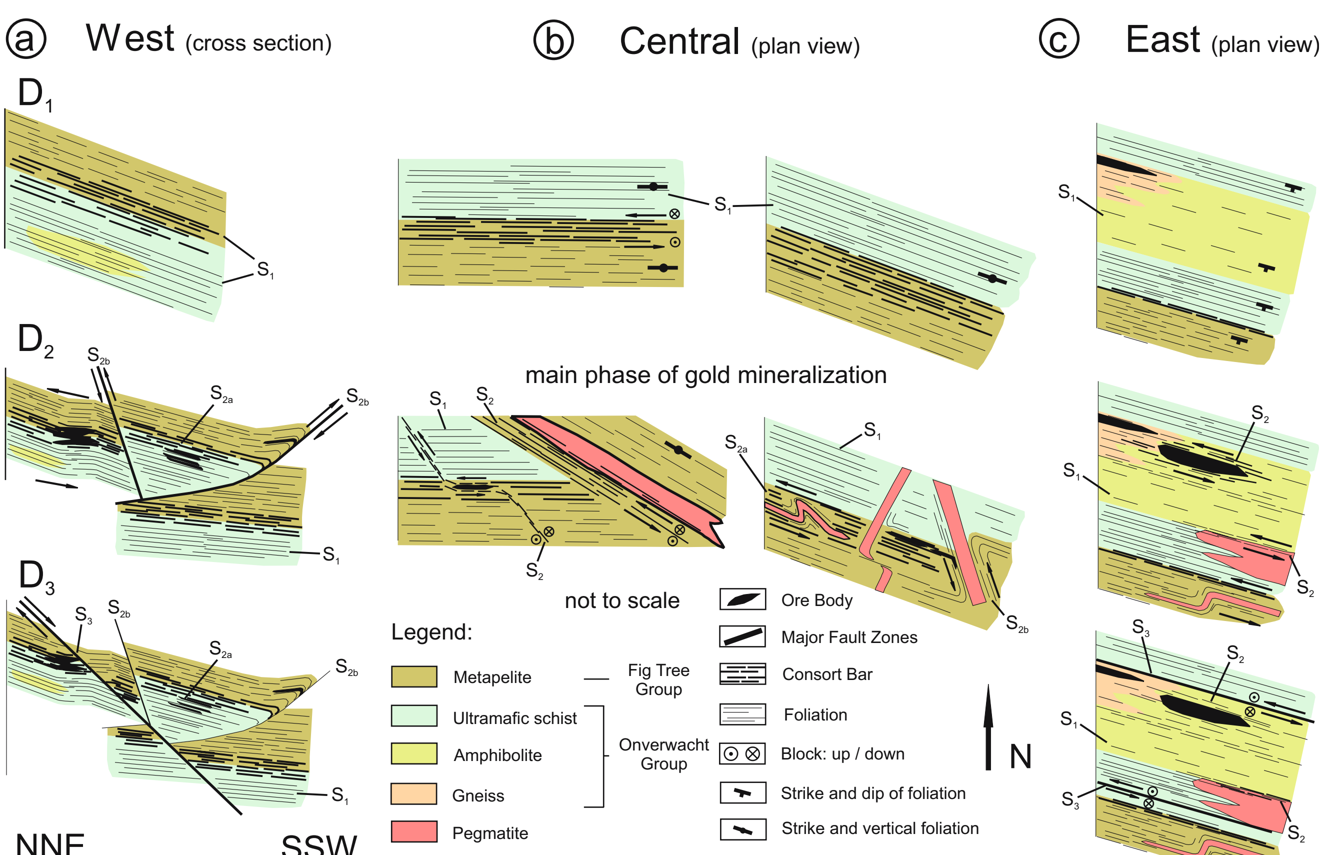

Fig. 4 Sketches illustrating the relative timing of deformation, mineralization, and magmatism in the **a** Western, **b** Central, and **c** Eastern Zones. *Line spacing* reflects the intensity of deformation in different rock types

defined by alteration minerals such as Cr-bearing muscovite, biotite, and tourmaline. Kinematic indicators, such as the displacement and duplication of the local stratigraphy, point to a reverse (top to the north) sense of movement. Conjugate sets of crosscutting reverse faults (S_{2b}) that dip at shallow to steep angles either to the N or S displace the mineralization. The gold mineralization is mainly hosted by centimeter- to decimeter- wide S_{2a}-parallel laminated quartz veins within the Consort Bar. The main ore body is located where the generally moderately SSW dipping S_{2a} foliation shows subhorizontal dips (Fig. 4a). The SE plunge of the ore bodies is at high angles to the mainly dip–slip movement along the shears, parallel to the fold axis of the three Shaft Syncline. The mineralized shoot is interpreted as being situated in the flat of a flat-and-ramp structure that acted as a preferred location for fluid flow and gold precipitation (Fig. 4a). The thickness of the ore bodies reaches up to c. 5 m, but for the most part, the mineralized horizons are only 1 to 2 m thick. D_3-related brittle normal faults dip at moderate angles to the SW and locally displace the ore bodies.

In the Central Zone, the S_1 foliation dips subvertically and strikes W–E to NW–SE (Fig. 4b). The Consort Bar varies in thickness between 0.5 and 20 m. The D_2 deformation is characterized by the development of several NW–SE trending, anastomosing shear zones of the SSZ, which crosscut the S_1 foliation. The kinematics of individual S_2 shear zones range from sinistral strike slip to an oblique reverse sense of shear, in agreement with subhorizontal to moderately N–NW plunging lineations. The foliation-parallel, steeply E and SE plunging ore bodies are c. 1.5×5 m in cross-section and strongly elongated, showing down-plunge extents in excess of c. 100 m. The main ore bodies are situated at the intersection of D_1 and D_2 shear zones where the D_2 shear zones are deflected (Fig. 4b). The kinematics in both ore bodies and D_2 shear zones are oblique sinistral strike slip, and thus, at high angles to the subvertical plunge of the ore bodies. This geometry and the kinematics of the

Table 1 Representative electron microprobe analyses of amphibole and plagioclase from amphibolites

	Hornblende Western Zone	Hornblende Eastern Zone		Plagioclase Western Zone	Plagioclase Eastern Zone
SiO_2	52.82	40.94	SiO_2	68.06	57.01
TiO_2	0.15	0.72	Al_2O_3	20.55	28.01
Al_2O_3	3.40	14.78	FeO	0.05	0.03
FeO	11.59	21.38	MnO	0.00	0.00
MnO	0.31	0.31	BaO	0.00	0.03
MgO	16.23	5.29	CaO	0.45	9.29
CaO	12.35	12.03	Na_2O	11.28	5.89
Na_2O	0.51	1.13	K_2O	0.02	0.15
K_2O	0.03	1.25	Total	100.41	100.39
Total	97.39	97.82			
TSi	7.57	6.27	Si	11.84	10.17
TAl	0.43	1.73	Al	4.21	5.88
TFe^{3+}	0.00	0.00	Fe^{2+}	0.01	0.00
TTi	0.00	0.00	Mn	0.00	0.00
CAl	0.14	0.94	Ba	0.00	0.00
CFe^{3+}	0.22	0.07	Ca	0.09	1.77
CTi	0.02	0.08	Na	3.81	2.04
CMg	3.47	1.21	K	0.00	0.03
CFe^{2+}	1.13	2.67	Cations	19.95	19.90
CMn	0.02	0.03			
CCa	0.00	0.00	X_{Ab}	0.97	0.53
BMg	0.00	0.00	X_{An}	0.03	0.46
BFe^{2+}	0.03	0.00	X_{Or}	0.00	0.01
BMn	0.02	0.01			
BCa	1.90	1.97			
BNa	0.06	0.01			
ACa	0.00	0.00			
ANa	0.09	0.32			
AK	0.01	0.24			
Cations	15.09	15.57			
X_{Mg}	0.75	0.31			

Structural formulas are based on 23 oxygen for amphibole and 32 oxygen for plagioclase.

intersecting shear zones suggest that the ore bodies are localized in dilational jogs that formed during deformation and intersection of the shear zone system (Fig. 4b). This type of mineralization locally forms massive sulfide bodies that are surrounded by a zone of disseminated sulfides. Only a small number of millimeter- to centimeter-scale quartz veins occur within the ore bodies. Abundant pegmatite dikes, which are folded and sheared along their margins, intruded parallel to the S_{2a} foliation. However, some pegmatites crosscut the S_1/S_{2a} foliation as well as the mineralization. They are also deformed along their margins (S_{2b}). D_3 normal faulting has not been observed.

In the Eastern Zone (Fig. 4c), the S_1 foliation dips at moderate angles to the SSW. Here, the Onverwacht Group comprises ultramafic schists, amphibolites, as well as intercalated gneisses that possibly represent former granites (Fig. 3). Minor intercalations of Fig Tree Group metapelites occur in the footwall of the Consort Bar, pointing to the tectonic imbrication of Fig Tree Group lithologies in the Onverwacht Group. Here, the thickness of the Consort Bar is c. 1 m. A first episode of disseminated, replacement style mineralization is characterized by a calcsilicate alteration assemblage in gneisses and amphibolites of the Onverwacht Group (Fig. 4c). The main stage of gold mineralization and hydrothermal alteration is related to centimeter- to decimeter-wide syn-kinematic (D_2) quartz veins. The emplacement geometries and progressive deformation of the quartz veins point to a predominantly sinistral strike-slip sense of movement. The up to several meters thick, elongate, and foliation-parallel ore bodies show subvertical plunges, and are, thus, perpendicular to the movement direction along the D_2 shear zones. The geometry is consistent with an origin as dilational jogs that developed during sinistral strike-slip shearing. However, large variations in the ore grade suggest a more irregular and complex geometry of the ore bodies. Up to several meters wide pegmatite dikes intruded syn-kinematically along the S_2 foliation. Intrusive contacts are clearly discernable, but the pegmatites are commonly mylonitized. Smaller pegmatite dikes are, in places, folded, and the asymmetry of folds points to a sinistral strike-slip sense of movement. The last deformation (D_3) is characterized by about 1 to 3 m wide brittle

Table 2 Representative electron microprobe analyses of garnet from metapelites

	Garnet/core Fig Tree WZ	Garnet/rim Fig Tree WZ	Garnet Fig Tree WZ	Garnet/core Fig Tree CZ	Garnet/rim Fig Tree CZ	Garnet/core Fig Tree EZ	Garnet/rim Fig Tree EZ	Garnet/core Onverwacht EZ	Garnet/rim Onverwacht EZ
SiO_2	37.02	36.92	37.15	37.04	37.22	36.49	36.48	37.15	37.66
TiO_2	0.06	0.08	0.02	0.00	0.00	0.02	0.00	0.07	0.00
Al_2O_3	20.22	20.62	21.04	21.06	21.14	21.96	21.91	20.74	21.08
Cr_2O_3	0.17	0.15	0.24	0.15	0.16	0.02	0.24	0.24	0.01
FeO	24.22	21.58	22.51	32.13	34.02	32.18	33.77	33.49	32.82
MnO	8.20	10.03	9.15	3.16	2.09	2.69	0.94	1.55	1.43
MgO	0.80	0.60	0.79	3.78	3.67	2.59	3.73	3.05	2.75
CaO	8.57	9.26	8.81	2.38	2.02	4.29	3.21	3.70	5.13
Na_2O	0.01	0.00	0.01	0.03	0.00	0.00	0.01	0.00	0.00
Total	99.26	99.24	99.72	99.73	100.32	100.24	100.28	99.98	100.89
TSi	3.00	2.99	2.99	2.97	2.97	2.92	2.90	2.98	2.99
TAl	0.00	0.01	0.01	0.03	0.03	0.08	0.10	0.02	0.01
Al VI	1.93	1.96	1.99	1.96	1.96	1.99	1.96	1.94	1.96
Fe^{3+}	0.04	0.03	0.00	0.06	0.05	0.11	0.11	0.05	0.04
Ti	0.00	0.01	0.00	0.00	0.00	0.00	0.00	0.00	0.00
Cr	0.01	0.01	0.02	0.01	0.01	0.00	0.02	0.02	0.00
Fe^{2+}	1.61	1.44	1.52	2.10	2.23	2.05	2.14	2.20	2.14
Mg	0.10	0.07	0.10	0.45	0.44	0.18	0.06	0.37	0.33
Mn	0.56	0.69	0.62	0.22	0.14	0.31	0.44	0.11	0.10
Ca	0.75	0.80	0.76	0.20	0.17	0.37	0.27	0.32	0.44
Na	0.00	0.00	0.00	0.00	0.00	0.00	0.00	0.00	0.00
Cations	8.00	8.00	8.00	8.00	8.00	8.00	8.00	8.00	8.00
X_{Alm}	0.53	0.48	0.51	0.71	0.75	0.70	0.73	0.74	0.72
X_{Grss}	0.22	0.25	0.25	0.04	0.03	0.07	0.03	0.08	0.13
X_{Pyp}	0.03	0.02	0.03	0.15	0.15	0.11	0.15	0.12	0.11
X_{Spss}	0.19	0.23	0.21	0.07	0.05	0.06	0.02	0.04	0.03

Structural formulas are based on 12 oxygen for garnet.
WZ Western Zone, *CZ* Central Zone, *EZ* Eastern Zone

faults. The lineations plunge at moderate angles to the SE. Kinematic indicators such as serpentine slickenfibers point to sinistral oblique-slip normal faulting.

Analytical procedures

Detailed petrological and mineral–chemical investigations were carried out to establish the metamorphic evolution of host rocks and the P–T conditions during hydrothermal alteration and gold mineralization. The chemical composition of minerals of the host rock, alteration, and ore assemblages was determined by a JEOL JXA-8900R electron microprobe at the Institute of Mineralogy and Economic Geology, RWTH Aachen University. The analyses were performed using natural mineral standards and wavelength dispersive spectrometers with an acceleration voltage age of 15 kV and a beam current of 23 nA for silicates, 15 kV and 20 nA for carbonates, and 25 kV and 28 nA for sulfides. All minerals were analyzed with a focused beam except for biotite, plagioclase, and carbonates. In these cases, the beam diameter was set to 5 to 10 μm, depending on the grain size. The data were corrected using the ZAF correction.

Mineral assemblages of host lithologies

Samples were taken from all major rock types, including Onverwacht Group amphibolites and ultramafic schists, intercalated gneisses, as well as Fig Tree Group metapelites.

Table 3 Representative electron microprobe analyses of biotite, plagioclase, and amphibole from metapelites

	Biotite Fig Tree WZ	Biotite Fig Tree CZ	Biotit Fig Tree EZ	Biotit Onverwacht EZ		Plagioclase Fig Tree CZ	Plagioclase/core Fig Tree EZ	Plagioclase/rim Fig Tree EZ		Hornblende Fig Tree WZ
SiO_2	36.20	37.05	36.63	35.97	SiO_2	58.21	53.10	57.41	SiO_2	41.72
TiO_2	1.09	1.54	1.59	1.61	Al_2O_3	27.16	29.93	27.96	TiO_2	0.14
Al_2O_3	18.26	18.00	18.20	17.78	FeO	0.25	0.20	0.19	Al_2O_3	16.25
Cr_2O_3	0.26	0.42	17.94	19.75	MnO	0.00	0.03	0.00	FeO	20.54
FeO	22.10	16.58	0.05	0.11	BaO	0.00	0.01	0.05	MnO	0.46
MnO	0.25	0.00	11.91	10.30	CaO	8.35	11.69	8.54	MgO	5.52
MgO	8.30	12.99	0.01	0.00	Na_2O	6.02	4.57	5.98	CaO	11.92
CaO	0.00	0.02	0.09	0.07	K_2O	0.05	0.06	0.03	Na_2O	0.81
Na_2O	0.07	0.10	9.37	9.95	Total	100.05	99.60	100.20	K_2O	0.70
K_2O	9.48	9.33	95.78	95.53					Total	98.06
Total	96.01	96.04								
			2.75	2.74	Si	10.38	9.64	10.24	TSi	6.27
Si	2.77	2.75	1.25	1.26	Al	5.70	6.40	5.87	TAl	1.73
Al IV	1.23	1.25	0.35	0.33	Fe^{2+}	0.04	0.03	0.03	TFe^{3+}	0.00
Al VI	0.41	0.33	0.09	0.09	Mn	0.00	0.01	0.00	TTi	0.00
Ti	0.06	0.09	1.13	1.26	Ba	0.00	0.00	0.00	CAl	1.15
Fe^{2+}	1.41	1.03	0.00	0.02	Ca	1.60	2.27	1.63	CFe^{3+}	0.27
Cr	0.02	0.03	1.33	1.17	Na	2.08	1.61	2.07	CTi	0.02
Mn	0.02	0.00	0.00	0.00	K	0.01	0.01	0.01	CMg	1.24
Mg	0.95	1.44	0.01	0.01	Cations	19.81	19.96	19.85	CFe^{2+}	2.30
Ca	0.00	0.00	0.90	0.97					CMn	0.03
Na	0.01	0.02	7.81	7.85	X_{Ab}	0.56	0.41	0.56	CCa	0.00
K	0.93	0.89			X_{An}	0.43	0.58	0.44	BMg	0.00
Cations	7.80	7.81	0.54	0.48	X_{Or}	0.00	0.00	0.00	BFe^{2+}	0.01
X_{Mg}	0.40	0.58							BMn	0.03
									ACa	0.00
									BNa	0.04
									ACa	0.00
									ANa	0.19
									AK	0.13
									Cations	15.33
									X_{Mg}	0.35

Structural formulas are based on 23 oxygen for amphibole, 32 oxygen for plagioclase, and 11 oxygen for biotite.
WZ Western Zone, *CZ* Central Zone, *EZ* Eastern Zone

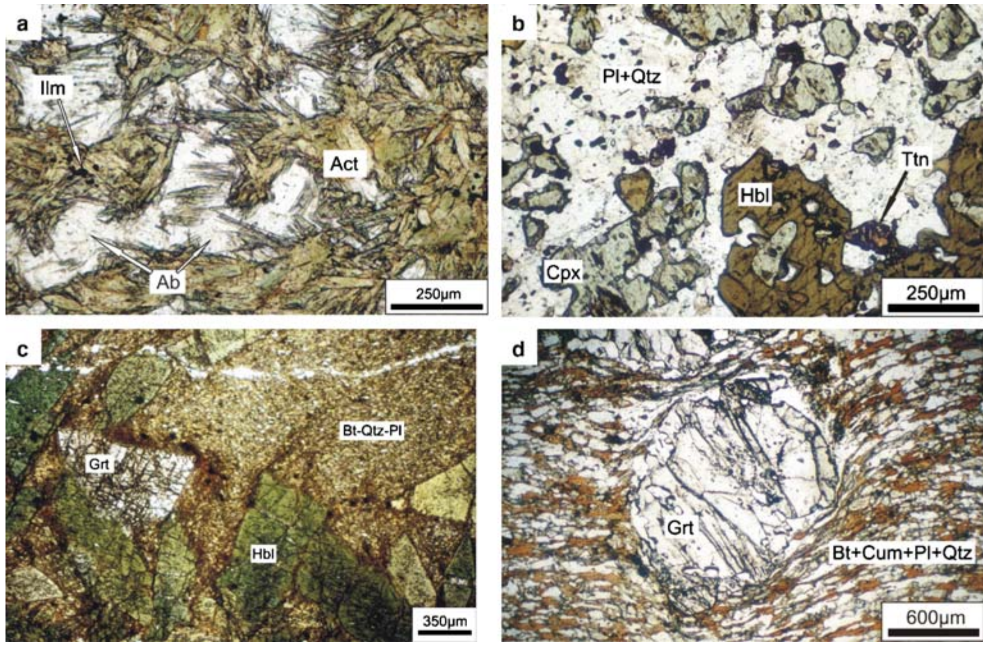

Fig. 5 Photomicrographs (plane-polarized light) showing representative mineral assemblages of host rocks. **a** Mafic rock of the Western Zone consisting of actinolite, albite, and minor ilmenite. **b** Amphibolite in the Eastern Zone consisting of hornblende, plagioclase, quartz, titanite, and clinopyroxene. **c** Metapelite of the Western Zone consisting of very fine-grained biotite–quartz–plagioclase matrix and porphyroblasts of hornblende and garnet. **d** Metapelite of the Eastern Zone comprising garnet porphyroblasts in a matrix of aligned biotite, cummingtonite, quartz, and plagioclase

Representative analyses for rock forming minerals are given in Tables 1, 2, and 3. Mineral abbreviations are after Kretz (1983).

Amphibolites

Onverwacht Group amphibolites occur as massive and relatively competent rocks that are aligned along the S_1 foliation. They are fine- to medium-grained, unfoliated to strongly schistose, and mainly consist of amphibole and plagioclase. In the Western Zone, the amphibolite is green in color and undeformed (Fig. 5a). The rock consists of amphibole, which ranges in composition from magnesio-hornblende to actinolite (Table 1), albite, quartz, and ilmenite. This assemblage, as well as the composition of amphibole, points to upper greenschist facies conditions. In contrast, the amphibolite in the Eastern Zone is commonly banded, dark greenish-gray in color, and exhibits a well-developed S_1 foliation, which is mainly defined by hornblende. The hornblende has a ferropargasitic composition (T_{Si} 5.9–6.4; X_{Mg} 0.30–0.35), and the associated plagioclase is andesine (X_{An} 0.40–0.47). Typical mineral assemblages include hornblende + plagioclase + quartz + ilmenite ± titanite, and hornblende + clinopyroxene + plagioclase + quartz + titanite ± calcite (Table 1; Fig. 5b), indicating amphibolite facies conditions.

Ultramafic schists

The ultramafic schists are dark greenish-gray, medium- to coarse-grained, and variably foliated. Elongate, up to several millimeters long, and commonly deformed tremolite is the most abundant phase in this rock. Individual grains grew along as well as across the foliation. Mineral assemblages of tremolite + serpentine + talc + magnetite are typical of ultramafic rocks in the Western Zone, indicating temperatures of c. 500°C (e.g., Spear 1993). Ultramafic rocks in the Central and Eastern Zones consist of tremolite + anthophyllite (cummingtonite) + forsterite + talc, pointing to distinctly higher temperatures above 600°C. In D_3 structures, these high-temperature assemblages have been completely replaced by serpentine + chlorite + magnesite + magnetite.

Gneiss

Gneiss has only been identified in the Eastern Zone. The fine- to medium-grained rock is leucocratic, locally reddish-brown in color, and has a well-developed S_1 foliation. The mineral assemblage is K-feldspar + plagioclase + quartz + biotite + muscovite ± titanite ± rutile.

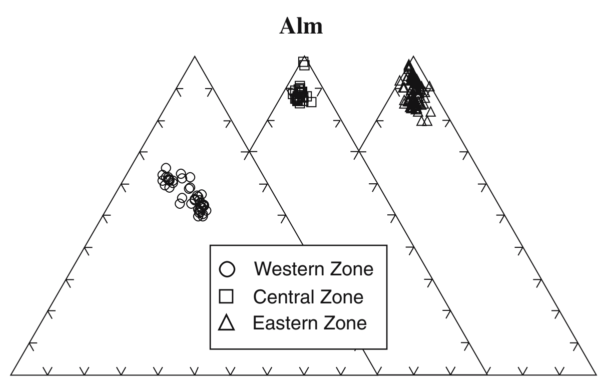

Fig. 6 Compositional variations in garnet from the metapelites of the Western, Central, and Eastern Zones

Metapelites

The Fig Tree Group metapelites are schistose to mylonitic. In the Western Zone, they are very fine-grained, with grain sizes ranging between 10 and 40 µm. The common mineral assemblage is biotite (X_{Mg} ~0.40) + quartz + plagioclase ± cummingtonite. Rare, up to 500 µm large garnet and hornblende porphyroclasts occur in layers that are relatively enriched in manganese and calcium (Fig. 5c). These layers do not exceed 1 cm in thickness and are associated with thin intercalations of garnet–grunerite–magnetite schists. Hornblende porphyroclasts are ferrotschermakite to ferro-hornblende (T_{Si} 6.1–6.9; X_{Mg} 0.33–0.43). The dominant garnet components are Alm, Grs, and Sps (Fig. 6). Garnet is slightly zoned from core to rim (Fig. 6; X_{Alm} 0.53$_{core}$–0.48$_{rim}$; X_{Grs} 0.22$_c$–0.25$_r$; X_{Sps} 0.19$_c$–0.23$_r$; X_{Pyr} ~0.03) and contains numerous inclusions of quartz, biotite, and cummingtonite (Fig. 5c). The metapelites in the Central and Eastern Zones are dark brown, predominantly fine-grained, and pervasively foliated. Common mineral assemblages include garnet + cummingtonite + biotite + quartz + plagioclase ± ilmenite, and cummingtonite + biotite + quartz + plagioclase ± ilmenite (Fig. 5d). The matrix consists of fine-grained biotite, quartz, plagioclase, and ilmenite. Syn- to post-tectonic garnet and/or cummingtonite occurs as up to several millimeter large porphyroblasts. Due to minor differences in bulk rock chemistry, the mineral chemistry of the rock forming minerals varies. In the Central Zone, biotite has X_{Mg} values between 0.57 and 0.62. The associated almandine garnet records a weak prograde growth zonation (X_{Alm} 0.71–0.75; X_{Grs} ~0.03; X_{Sps} 0.17–0.11; X_{Pyr} ~0.15), while plagioclase is andesine (X_{Ab} 0.40–0.44). Biotite in metapelites of the Eastern Zone has slightly lower X_{Mg} values (0.50–0.57). Here, plagioclase is

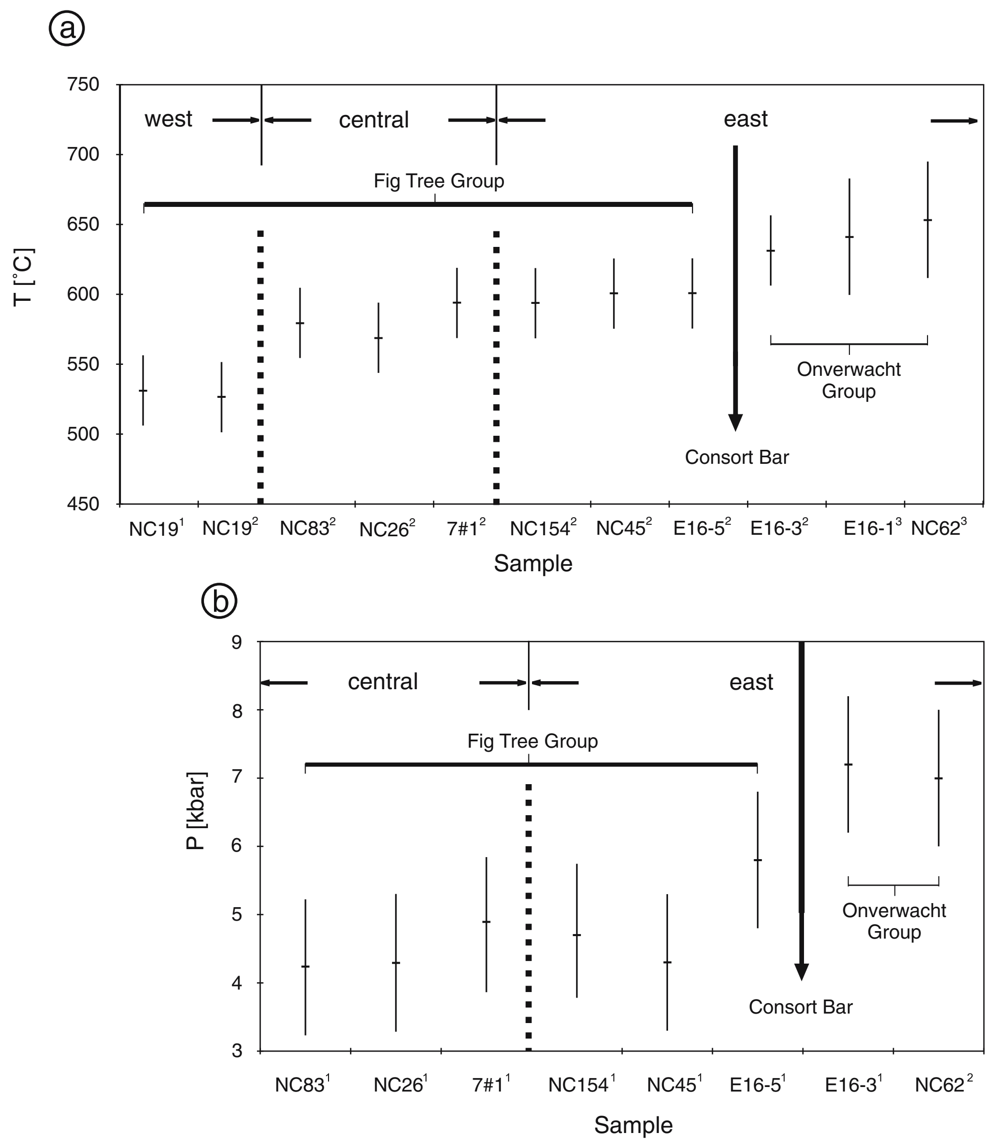

Fig. 7 Diagram summarizing the estimated peak metamorphic **a** temperature and **b** pressure conditions of host lithologies at the New Consort Gold Mine. The error bars are ±25°C for the temperature and ±1 kbar for the pressure estimation. West, Central, East correspond to the three investigated areas. The calibrations used for estimating the peak temperatures include the [1]Grt–Hbl (Ravna 2000a), [2]Grt–Bt (Holdaway 2000), and [3]Hbl–Pl thermometers (Holland and Blundy 1994). Pressure estimates are based on the [1]Grt–Bt–Pl–Qtz and [2]Hbl–Pl barometers of Wu et al. (2004) and Plyusnina (1982), respectively

zoned from core to rim (X_{An} 0.58$_c$–0.44$_r$), while garnet is compositionally similar to those of the Central Zone (X_{Alm} 0.70–0.73; X_{Grs} 0.07–0.03; X_{Sps} 0.06–0.02; X_{Pyr} 0.11–0.15; Figs. 5d and 6). Metapelites in the footwall of the Consort Bar are more uniform and consist of garnet (X_{Alm} 0.74; X_{Grs} 0.08; X_{Sps} 0.04; X_{Pyr} 0.12), plagioclase (X_{An} 0.40–0.50), quartz, biotite (X_{Mg} 0.46–0.49), and ilmenite.

Metamorphic conditions

Several conventional geothermometers and geobarometers were applied to suitable mineral assemblages in unaltered metapelites and amphibolites. The application of the average PT method using THERMOCALC (Holland and Powell 1998) was not successful due to the lack of suitable mineral assemblages. The applied methods include the garnet–biotite (Holdaway 2000), garnet–hornblende (Ravna 2000a), and hornblende–plagioclase (Holland and Blundy 1994) thermometers, as well as the hornblende–plagioclase and garnet–biotite–plagioclase–quartz barometers of Plyusnina (1982) and Wu et al. (2004). The results (Fig. 7, Table 4) confirm the presence of a steep metamorphic gradient in the mine.

Within the Fig Tree Group metapelites in the hanging wall of the Consort Bar, the data indicate a systematic increase in peak temperatures from the structurally highest Western Zone to the structurally deepest Eastern Zone (Fig. 7a). In the Western Zone, the estimated temperatures are at 520±25°C. In the Central and Eastern Zones, temperatures of c. 570±25°C and 590±25°C indicate distinctly higher metamorphic conditions. The associated pressures of c. 4–5 kbar are equivalent to a crustal depth of c. 15–17 km during the peak of metamorphism in the hanging wall of the Consort Bar (Fig. 7b).

In contrast, P–T estimates on Onverwacht Group amphibolites and intercalated metapelites in the footwall of the Consort Bar (Eastern Zone) reveal distinctly higher metamorphic conditions of c. 600–700°C and 6–8 kbar (Fig. 7a,b). These estimates point to a difference in peak-pressures of up to 3 kbar recorded in rocks below and above the Consort Bar, suggesting that a crustal column of up to 10 km may have been excised along this structural contact. It is this structural excision of strata that is largely responsible for the observed telescoping of metamorphic conditions. These higher P–T conditions are also consistent with the high-temperature (>600°C) mineral assemblages observed in Onverwacht Group ultramafic schists in the Central and Eastern Zones. Unfortunately, P-estimates in these rocks were not possible due to the lack of pressure-sensitive mineral equilibria. Onverwacht Group rocks in the Western Zone do not indicate similarly high P–T conditions. This may indicate that the ultramafic units of the Onverwacht Group below the Consort Bar are also tectonically imbricated, rather than representing a seemingly homogeneous and largely undisturbed stratigraphic succession.

Table 4 Summary of mineral assemblages, mineral chemistry, and PT estimations of the New Consort Gold Mine

	Rock type	Mineral assemblage	Mineral chemistry	Geothermometer	Estimated PT conditions
Western Zone	Metapelite	Bt–Qtz ± Pl ± Grt ± Hbl	Garnet: X_{Alm} 0.53–0.48 X_{Grs} 0.22–0.25 X_{Sps} 0.19–0.23 X_{Pyr} ~0.03	Grt–Bt[a]	530±25°C
			Biotite: X_{Mg} ~0.40	Grt–Hbl[d]	510±25°C
			Hornblende: T_{Si} 6.2–6.7 X_{Mg} 0.33–0.43		
Central Zone	Metapelite	Grt–Bt–Cum–Pl–Qtz ± Ilm	Garnet: X_{Alm} 0.71–0.75 X_{Grs} ~0.03 X_{Sps} 0.17–0.11 X_{Pyr} ~0.15	Grt–Bt–Pl–Qtz[a,b]	570±25°C at 4.5±1 kbar
			Biotite: X_{Mg} 0.57–0.62		
			Plagioclase: X_{An} 0.40–0.44		
Eastern Zone	Amphibolite	Hbl–Pl–Qtz–Ttn ± Ilm ± Cpx ± Ep	Hornblende: T_{Si} 5.9–6.4 X_{Mg} 0.30–0.35	Hbl–Pl[c]	660±40°C
			Plagioclase: X_{An} 0.40–0.47		
	Metapelite (Onverwacht)	Grt–Bt–Pl–Qtz ± Ilm	Garnet: X_{Alm} 0.74 X_{Grs} 0.08 X_{Sps} 0.04 X_{Pyr} 0.12	Grt – Bt – Pl – Qtz[a,b]	630±25°C at 7.2±1 kbar
			Biotite: X_{Mg} 0.46–0.49		
			Plagioclase: X_{An} 0.40–0.50		
	Metapelite (Fig Tree)	Grt–Bt–Cum–Pl–Qtz ± Ilm	Garnet: X_{Alm} 0.70–0.73 X_{Grs} 0.07–0.03 X_{Sps} 0.06–0.02 X_{Pyr} 0.11–0.15	Grt–Bt–Pl–Qtz[a,b]	590±25°C at 4.9±1 kbar
			Biotite: X_{Mg} 0.50–0.57		
			Plagioclase: X_{An} 0.58–0.44		

[a] Calibrations are from Holdaway (2000).
[b] Calibrations are fromWu et al. (2004).
[c] Calibrations are from Holland and Blundy (1994).
[d] Calibrations are from Ravna (2000a).

Veins and wall rock alteration

The different ore bodies in the Western, Central, and Eastern Zones are associated with distinct alteration zones, which vary in mineralogy depending on (1) the original mineralogy of the respective host lithology, (2) the temperature at which mineralization occurred, as well as (3) fluid–rock ratios. Sketches illustrating the characteristics of ore bodies/alteration zones are shown in Fig. 8, and examples of representative alteration assemblages are given in Fig. 9.

Western Zone

The mineralized Consort Bar in the Western Zone has a characteristic green color due to the predominance of Cr-bearing muscovite. The mineralization is associated with (S_{2a}) parallel laminated quartz veins that occur over a total distance of about 1.5 m (Fig. 8a). The proximal alteration is restricted to the mylonites that enclose individual millimeter- to decimeter-wide quartz veins. The proximal alteration assemblage comprises quartz, Cr-bearing muscovite, K-feldspar (Fig. 9a), plagioclase, and biotite. Cr-bearing muscovite and biotite are aligned along the S_2 foliation. The distal alteration extends up to 4 m into the wall rocks. In the ultramafic schists immediately below the mineralized Consort Bar, it comprises calcite, dolomite, biotite, tourmaline, and Cr-bearing muscovite. Fine-grained biotite and up to 500 μm large and commonly boudinaged tourmaline often occur in microscopic D_2 shear zones that are parallel to the S_2 foliation. In other places, biotite and tourmaline replaced peak metamorphic tremolite (Fig. 9b). The mineralization in metapelites is associated with abundant micrometer- to centimeter-thick and often deformed quartz–sulfide veins. They display different orientations, but are mostly parallel to slightly oblique to S_2. The different

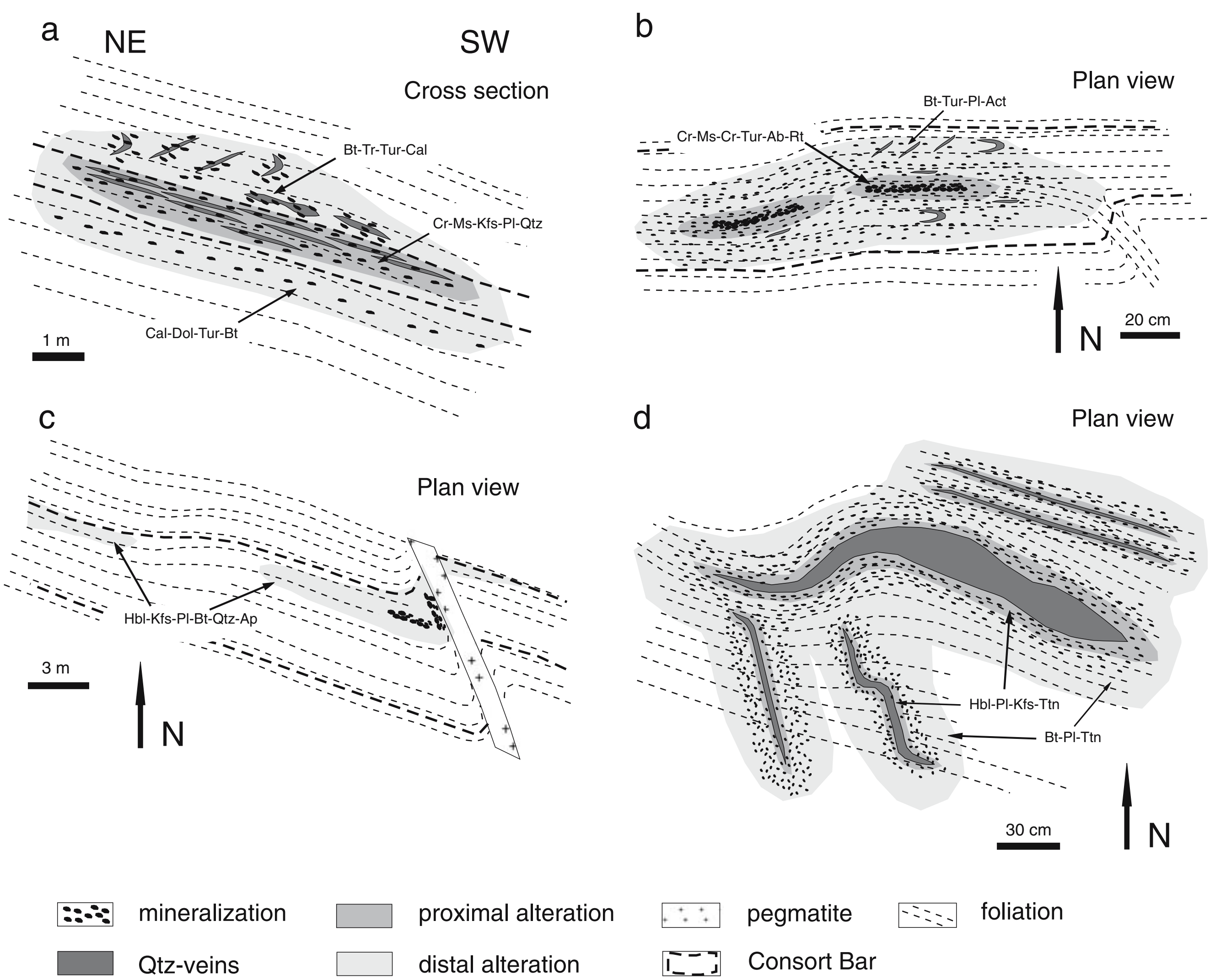

Fig. 8 Sketches illustrating the major characteristics of gold mineralization and alteration in the **a** Western, **b**, **c** Central, and **d** Eastern Zones

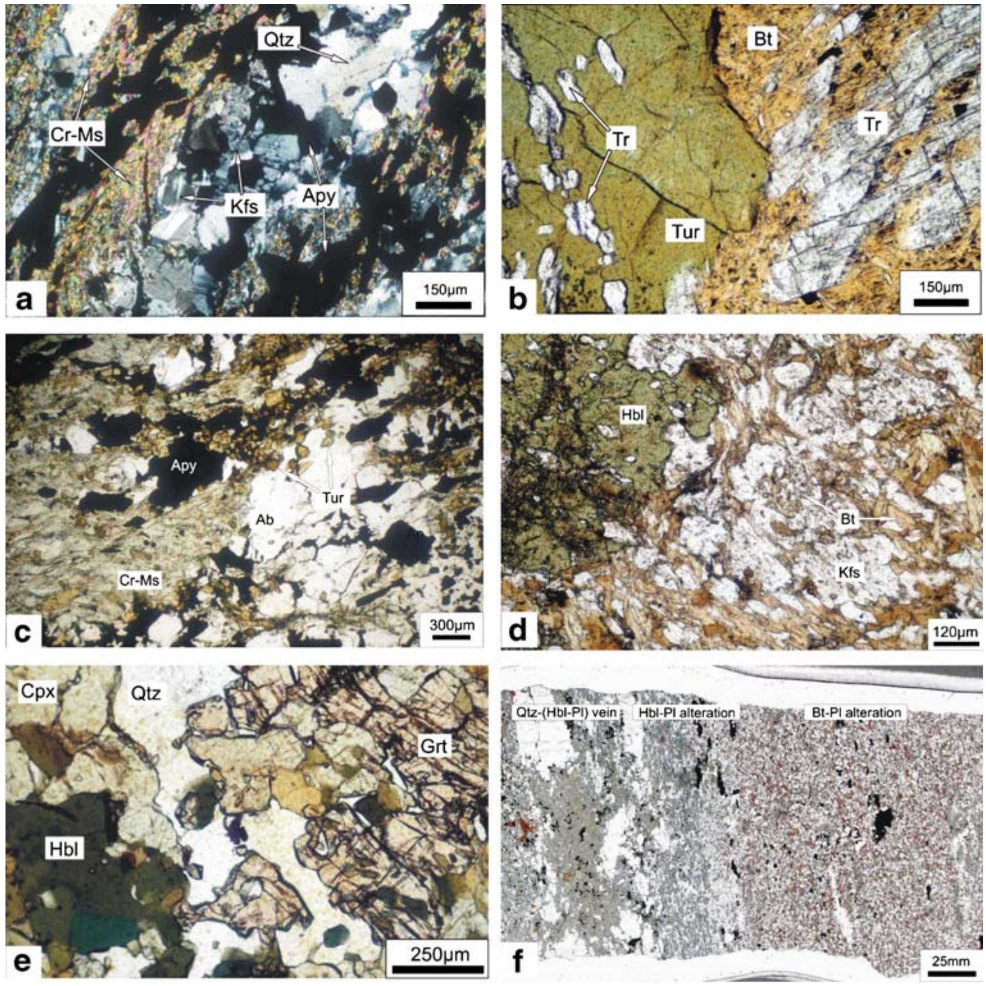

Fig. 9 Photomicrographs showing typical alteration assemblages associated with the mineralization. **a** Close-up of proximal Cr-bearing muscovite–K–feldspar–quartz alteration assemblage associated with laminated quartz veins (Western Zone; crossed-polarized light). **b** Example of distal biotite–tourmaline alteration assemblage replacing tremolite in ultramafic schists (Western Zone, plane-polarized light). **c** Proximal alteration zone of the Central Zone type I mineralization (plane-polarized light) consisting of albite, chromian tourmaline, Cr-bearing muscovite, and sulfides. **d** Type II alteration assemblage in the Central Zone (plane-polarized light) comprising of hornblende, biotite, and K-feldspar. **e** Early calc–silicate alteration assemblage of the Eastern Zone (plane-polarized light), comprising clinopyroxene, hornblende, garnet, and quartz. **f** Alteration zoning associated with extension veins of the late mineralization in the Eastern Zone (plane-polarized light) comprising a proximal hornblende–plagioclase and a distal biotite–plagioclase alteration zone

orientations are interpreted to have resulted from progressive rotation during shearing. In the immediate hanging wall of the Consort Bar, the alteration assemblage comprises biotite, tourmaline, tremolite, and carbonates. Metapelites containing quartz–sulfide veins further away from the main ore bodies do not show any evidence of hydrothermal alteration.

Central Zone

In the Central Zone, two different types of mineralization can be distinguished, which will be referred to as types I and II (Fig. 8b,c). These are interpreted to have formed contemporaneously. In both types, the style of mineralization is disseminated, and quartz veins are rare. The type I mineralization occurs in the western part of the Central Zone and is mineralogically similar to that of the Western Zone. The type II mineralization is restricted to the eastern part of the Central Zone, and the ore and alteration assemblages share many characteristics with those of in the Eastern Zone (Fig. 8c,d, and below).

The type I mineralization shows a distinct change of alteration assemblages with distance from the ore body (Fig. 8b). The proximal alteration zone is dominated by coarse-grained sulfides that are intergrown with chromian tourmaline, Cr-bearing muscovite, albite, and minor amounts of Cr-bearing spinel and rutile. This c. 5-cm thick massive zone is surrounded by a strongly foliated c. 0.5 m wide zone with a similar but finer grained alteration assemblage dominated by Cr-bearing muscovite (Fig. 9c). The distal alteration zone of type I ore bodies is characterized by pale-green medium-grained amphibole that can be classified as magnesiohornblende and actinolite (T_{Si} 7.2–7.9; X_{Mg} 0.79–0.86). It is associated with variable amounts of fine-grained tourmaline, biotite, and plagioclase (X_{An} 0.22–0.39; Table 5).

The type II mineralization does not exhibit distinct proximal and distal alteration zones. Here, the altered wall rocks are characterized by a continuous decrease in the abundance of alteration minerals with increasing distance from the ore body. The hydrothermal alteration comprises biotite, quartz, apatite, K-feldspar, hornblende, tourmaline, and titanite, along with disseminated sulfides (Fig. 9d). The

Table 5 Representative electron microprobe analyses of alteration assemblages

	Plagioclase CZ Type I	Plagioclase EZ Type II	Plagioclase EZ Type II		Hornblende CZ Type I	Hornblende EZ Type I	Hornblende EZ Type II		Garnet EZ Type I		Clinopyroxene EZ Type I
SiO_2	60.19	59.48	60.47	SiO_2	51.31	39.70	49.43	SiO_2	37.28	SiO_2	49.59
Al_2O_3	25.33	26.11	25.44	TiO_2	0.37	0.62	0.45	TiO_2	0.11	TiO_2	0.03
FeO	0.14	0.12	0.03	Al_2O_3	6.72	12.69	7.55	Al_2O_3	20.05	Al_2O_3	0.45
MnO	0.01	0.00	0.03	FeO	8.99	25.72	13.65	Cr_2O_3	0.05	FeO	20.50
BaO	0.00	0.00	0.00	MnO	0.72	0.38	0.74	FeO	23.49	MnO	0.43
CaO	6.47	7.19	6.40	MgO	16.21	3.64	12.69	MnO	3.09	MgO	5.53
Na_2O	7.37	7.04	7.25	CaO	11.75	11.78	11.72	MgO	0.53	CaO	23.26
K_2O	0.03	0.11	0.25	Na_2O	0.75	0.90	0.75	CaO	15.07	Na_2O	0.19
Total	99.53	100.04	99.87	K_2O	0.09	1.81	0.28	Na_2O	0.03	K_2O	0.00
				Total	96.90	97.23	97.25	Total	99.70	Total	99.96
Si	10.72	10.58	10.75	TSi	7.32	6.27	7.21	TSi	2.97	TSi	1.96
Al	5.32	5.47	5.33	TAl	0.68	1.73	0.79	TAl	0.03	TAl	0.02
Fe^{2+}	0.04	0.02	0.00	TFe^{3+}	0.00	0.00	0.00	Al VI	1.86	TFe^{3+}	0.00
Mn	0.00	0.00	0.00	TTi	0.00	0.00	0.00	Fe^{3+}	0.15	M1Al	0.00
Ba	0.00	0.00	0.00	CAl	0.45	0.63	0.51	Ti	0.01	M1Ti	0.00
Ca	1.24	1.37	1.22	CFe^{3+}	0.24	0.33	0.18	Cr	0.00	$M1Fe^{3+}$	0.00
Na	2.56	2.43	2.50	CTi	0.04	0.07	0.05	Fe^{2+}	1.42	$M1Fe^{2+}$	0.67
K	0.01	0.02	0.06	CMg	3.45	0.86	2.76	Mn	0.06	M1Mg	0.33
Cations	19.89	19.90	19.86	CFe^{2+}	0.78	3.07	1.45	Mg	0.21	M2Mg	0.00
				CMn	0.04	0.05	0.05	Ca	1.29	$M2Fe^{2+}$	0.01
X_{Ab}	0.67	0.64	0.66	CCa	0.00	0.00	0.00	Na	0.01	M2Mn	0.01
X_{An}	0.33	0.35	0.32	BMg	0.00	0.00	0.00	Cations	8.00	M2Ca	0.99
X_{Or}	0.00	0.01	0.02	BFe^{2+}	0.05	0.00	0.03			M2Na	0.01
				BMn	0.04	0.00	0.05	X_{Alm}	0.47	M2K	0.00
				BCa	1.80	1.99	1.83	X_{Grss}	0.36	Cations	4.00
				BNa	0.10	0.00	0.09	X_{Pyp}	0.02		
				ACa	0.00	0.00	0.00	X_{Spss}	0.07	X_{Mg}	0.32
				ANa	0.10	0.27	0.12				
				AK	0.02	0.37	0.05				
				Cations	15.11	15.64	15.17				
				X_{Mg}	0.80	0.22	0.65				

Structural formulas are based on 32 oxygen for plagioclase, 23 oxygen for amphibole, 12 oxygen for garnet, and 6 oxygen for clinopyroxene.
CZ Central Zone, *EZ* Eastern Zone

average width of the alteration extends about 5 m into the wall rocks.

Eastern Zone

In similarity with the Central Zone, two types of mineralization have been identified in the Eastern Zone, which differ in their mineralogy and style of alteration. However, the two types appear to be associated with distinctly different T-conditions during their formation, and previous studies have documented overprinting relationships (Tomkinson and Lombard 1990; and below). Thus, these types will be referred to as “early” and “late” mineralization. The early mineralization is associated with a distinct high-T calc–silicate alteration assemblage made up of clinopyroxene, amphibole, garnet, K-feldspar, quartz, calcite, biotite, and rare titanite (Fig. 9e). The rocks have a banded appearance, consisting of ca. 1 cm thick pale green bands of medium-grained hedenbergite (X_{Mg} ~0.32) containing sulfide and silicate inclusions and thin dark green laminae dominated by ferropargasite (T_{Si} 5.9–6.5; X_{Mg} 0.10–0.22; Table 5). Grossular–almandine garnet (X_{Alm} 0.47; X_{Grs} 0.36; X_{Sps} 0.07; X_{Pyr} 0.02), K-feldspar, quartz, biotite, and calcite are intergrown with hedenbergite and ferropargasite (Fig. 9e).

The late mineralization in the Eastern Zone is associated with centimeter- to decimeter-wide quartz veins (Fig. 8d). The quartz veins contain only small amounts of sulfides together with calcic amphibole of magnesiohornblende composition (T_{Si} 6.3–7.7; X_{Mg} 0.60–0.75), biotite, apatite, plagioclase (X_{An} 0.32–0.36), K-feldspar, and titanite (Table 7). The alteration assemblages in the wall rocks are subdivided into a proximal magnesiohornblende–plagioclase–K–feldspar–titanite alteration zone and a distal biotite–plagioclase–titanite alteration zone (Fig. 9f). Both alteration zones contain small amounts of calcite and epidote-group minerals.

Ore mineralogy

The alteration zones of the different ore bodies described above are associated with different ore parageneses (Fig. 10). In the Western Zone, the ore assemblage is dominated by arsenopyrite, pyrite, pyrrhotite, chalcopyrite, and gold (Fig. 10a,b). Minor phases include ullmannite, stibnite, and native antimony. Euhedral up to several hundred micrometers large arsenopyrite is the most abundant sulfide mineral. It commonly shows an oscillatory zoning. Pyrrhotite and chalcopyrite mainly occur at arsenopyrite grain boundaries. More rarely, arsenopyrite is intergrown with pyrite and pyrrhotite (Fig. 10a). In the overlying metapelites, the mineralization is characterized by coarse-grained arsenopyrite, pyrite, and pyrrhotite. Here, pyrite and pyrrhotite may also occur as fracture fillings in arsenopyrite. Gold is always associated with the sulfides and is not restricted to specific rock types. Native gold grains occur as inclusion in arsenopyrite (Fig. 10e), intergrown with sulfides (Fig. 10b), and as fracture fillings in vein, alteration, and ore minerals.

Table 6 Representative electron microprobe analyses of arsenopyrite

	Core WZ	Rim WZ	CZ	CZ	EZ	EZ
As	42.92	46.50	48.45	46.13	48.78	45.48
Ag	0.00	0.05	0.07	0.05	0.00	0.07
S	21.21	19.26	18.06	19.46	17.59	19.69
Au	0.06	0.00	0.00	0.00	0.00	0.09
Fe	34.77	34.22	32.65	33.81	33.42	33.97
Ni	0.02	0.05	0.77	0.16	0.06	0.11
Cu	0.00	0.00	0.00	0.00	0.00	0.00
Co	0.14	0.32	0.10	0.05	0.18	0.25
Total	99.12	100.39	100.10	99.66	100.03	99.66
at.%						
As	30.80	33.72	35.73	33.61	36.12	33.05
Ag	0.00	0.02	0.04	0.03	0.00	0.03
S	35.57	32.63	31.13	33.13	30.45	33.44
Au	0.02	0.00	0.00	0.00	0.00	0.03
Fe	33.47	33.29	32.30	33.04	33.20	33.12
Ni	0.02	0.04	0.72	0.14	0.06	0.10
Cu	0.00	0.00	0.00	0.00	0.00	0.00
Co	0.12	0.29	0.09	0.05	0.17	0.23

WZ Western Zone, *CZ* Central Zone, *EZ* Eastern Zone

Table 7 Summary of the ore and alteration assemblages and estimations of temperature of the mineralization in the New Consort Gold Mine

	Ore type	Ore assemblage	Alteration — proximal	Alteration — distal	Mineral chemistry	Geothermometer	Estimated T conditions
West	Consort Bar	Apy–Po–Cp–Ulm ± Stbn ± Sb	Cr–Ms–Kfs–Pl–Qtz ± Bt	Cal–Dol–Tur–Bt	Arsenopyrite: As (at.%) 32.5–34.7	Apy[a]	510±30°C
	Metapelite	Apy–Py–Po–Cp	Bt–Tur–Tr–Cal				
Central	Type I	Apy–Po–Cp ± Py	Cr–Tur–Cr–Ms–Ab ± Rt ± Cr–Spi	Act/Hbl–Tur–Pl–Bt	Hornblende: T_{Si} 7.0–7.8 X_{Mg} 0.79–0.86 Plagioclase: X_{An} 0.22–0.39	Hbl–Pl[b]	540±40°C
	Type II	Apy–Lol–Po ± Bi ± Mal	Hbl–Kfs–Pl–Bt–Qtz ± Tur ± Ttn				
East	early	Lol–Po	Cpx–Hbl ± Grt ± Kfs ± Qtz ± Bt ± Cal		Garnet: X_{Alm} 0.47 X_{Grs} 0.36 X_{Sps} 0.07 X_{Pyr} 0.02	Grt–Hbl[c]	690±25°C
					Clinopyroxene: X_{Mg} ~0.32 Hornblende: T_{Si} 5.9–6.5 X_{Mg} 0.10–0.22	Grt–Cpx [d,e,f]	670±25°C
	late	Apy–Lol–Po ± Cp	Hbl–Pl–Kfs–Ttn ± Ap ± Cal ± Ep	Bt–Pl–Ttn ± Kfs ± Ap ± Cal ± Ep	Hornblende: T_{Si} 6.4–7.7 X_{Mg} 0.6–0.75 Plagioclase: X_{An} 0.32–0.36	Hbl–Pl[b]	590±40°C

[a] Calibrations are from Sharp et al. (1985).
[b] Calibrations are from Holland and Blundy (1994).
[c] Calibrations are from Ravna (2000a).
[d] Calibrations are from Ravna (2000b).
[e] Calibrations are from Krogh (1988).
[f] Calibrations are from Sengupta et al. (1989).

The type I mineralization in the Central Zone is dominated by arsenopyrite, pyrrhotite, chalcopyrite, and gold. Locally, the sulfides are replaced by subhedral pyrite. The coarse-grained sulfides in the center of type I ore bodies are dominated by up to several millimeters large blocky crystals of arsenopyrite. Pyrrhotite and chalcopyrite occur at arsenopyrite grain boundaries as well as fracture fillings in arsenopyrite and alteration minerals. In the strongly foliated margins of the ore bodies, fine-grained needles of arsenopyrite and minor pyrrhotite are aligned along S_2. Gold occurs as inclusions in arsenopyrite, along grain boundaries and triple points between sulfides and alteration minerals, and in association with pyrrhotite along fractures in arsenopyrite and alteration minerals. The type II mineralization in the Central Zone contains disseminated, euhedral arsenopyrite that encloses anhedral loellingite (Fig. 10c). Gold, native bismuth, and maldonite occur as <10 µm large inclusions in arsenopyrite and loellingite. Arsenopyrite is the most abundant sulfide mineral in these rocks and is accompanied by pyrrhotite and chalcopyrite. Locally, arsenopyrite is replaced by pyrrhotite.

The early mineralization in the Eastern Zone is not associated with arsenopyrite. The ore assemblage comprises loellingite and pyrrhotite, which are intergrown with the calcsilicate alteration assemblage. Along fractures, small amounts of chalcopyrite and arsenopyrite have been identified. The late mineralization in the Eastern Zone is dominated by arsenopyrite, loellingite, pyrrhotite, and chalcopyrite. The sulfides are disseminated within the proximal and distal alteration zones. Only small amounts of sulfides occur within the quartz veins. Arsenopyrite forms coarse-grained subhedral to euhedral crystals. The arsenopyrite often contains inclu-

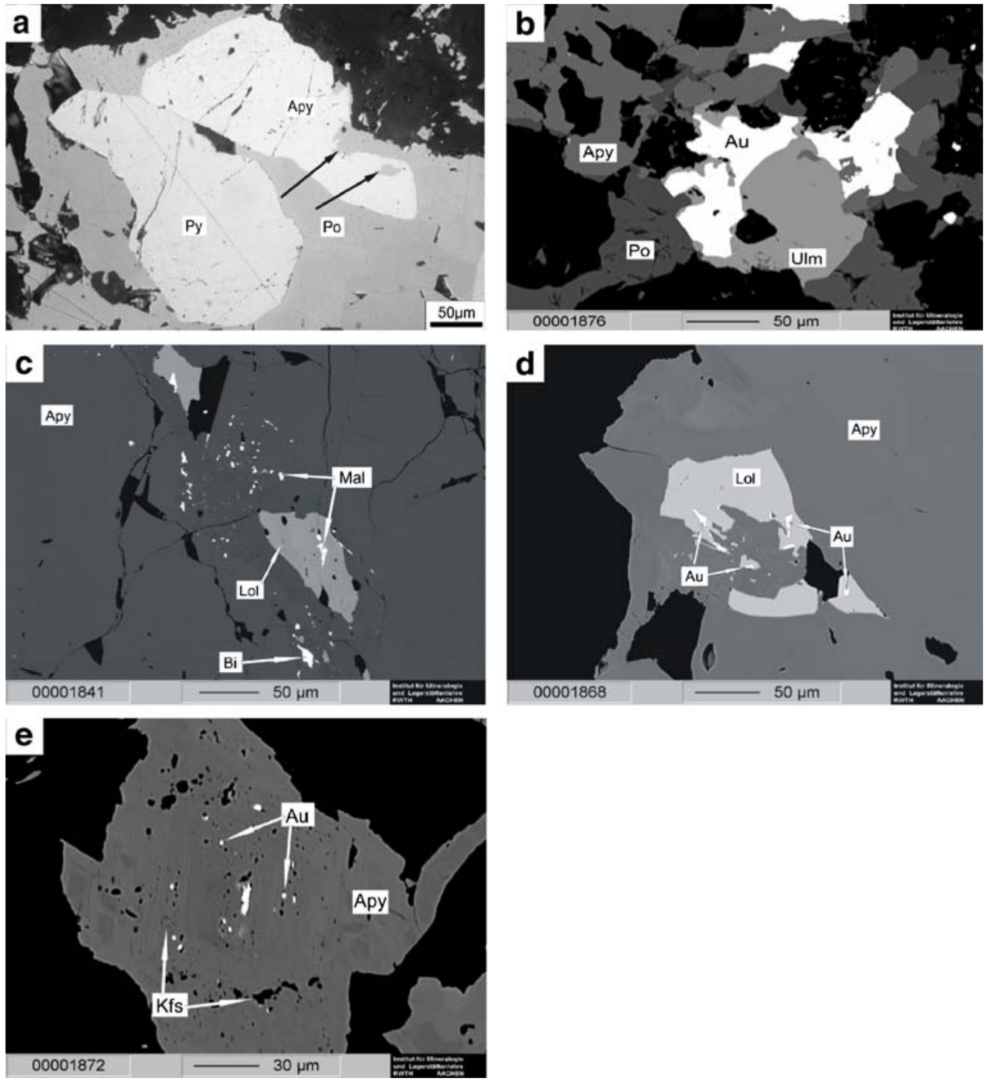

Fig. 10 **a** Photomicrograph (reflected light) and **b**–**e** back-scattered electron images showing representative ore assemblages. **a** Texturally equilibrated arsenopyrite–pyrite–pyrrhotite assemblage of the Western Zone. *Arrows* indicate replacement of arsenopyrite by pyrrhotite. **b** Gold intergrown with ullmannite, arsenopyrite, and pyrrhotite in the auriferous Consort Bar in the Western Zone **c** Arsenopyrite from the type II mineralization of the Central Zone containing inclusions of loellingite, maldonite, and native bismuth. **d** Relict loellingite with gold inclusions replaced by arsenopyrite (late mineralization in the Eastern Zone). **e** Arsenopyrite showing an oscillatory zoning with inclusions of gold and K-feldspar from the Western Zone

sions of loellingite and pyrrhotite (Fig. 10d). Gold occurs as inclusion in arsenopyrite, along loellingite–arsenopyrite (-pyrrhotite) boundaries, intergrown with sulfides, and as rare high-grade gold pockets within the quartz veins.

Temperatures of mineralization

The temperature conditions during mineralization were estimated using suitable ore and alteration assemblages. As the ore assemblages are dominated by Fe–As–S associations, the arsenopyrite geothermometer (Sharp et al. 1985) might be useful for estimating temperatures of mineralization for the different ore bodies. However, there is a large spread in Fe/As ratios in arsenopyrites of the different ore bodies and a considerable overlap between the different zones. This is due to the fact that the arsenic content in arsenopyrite is highly sensitive to changing sulfur fugacities (Sharp et al. 1985). A buffering sulfide assemblage is only present in the Western Zone where the arsenopyrite–pyrite–pyrrhotite assemblage is in textural equilibrium (Fig. 10a). The compositional range of arsenopyrite in contact with pyrite and pyrrhotite varies between 32.5 and 34.7 at.%, corresponding to a temperature of 510±30°C (Table 6).

The geothermometers chosen to estimate the temperature conditions during mineralization in the Central and Eastern Zones include the hornblende–plagioclase (Holland and Blundy 1994), garnet–hornblende (Ravna 2000a), and garnet–clinopyroxene (Ravna 2000b) thermometers. Hornblende–plagioclase pairs of the type I mineralization of the Central Zone reveals temperatures of 540±40°C. In contrast, garnet–hornblende and garnet–clinopyroxene pairs from the early mineralization in the Eastern Zone indicate distinctly higher temperatures of 680±25°C, pointing to upper amphibolite facies conditions. Alteration assemblages of the late mineralization in the Eastern Zone reveal considerably lower metamorphic conditions of 590±40°C (hornblende–plagioclase; Holland and Blundy 1994).

Discussion and conclusion

The synthesis of the structural data and petrological characteristics of metamorphic, ore, and alteration assemblages allows to evaluate the overall tectono-metamorphic evolution of the host rocks and the relative timing and conditions of gold mineralization. Peak metamorphic conditions of the wall rocks indicate a steep apparent metamorphic gradient in the mine. Such condensed metamorphic gradients are a characteristic feature of the granitoid–greenstone contacts in the Barberton Mountain Land and many other Archaean granite–greenstone terrains worldwide, and have been interpreted as a result of extensional detachment shearing and solid state doming at the base of the greenstone sequence (de Ronde and de Wit 1994; Kisters et al. 2003; Diener et al. 2005; Dziggel et al. 2006). At the New Consort Gold Mine, the metamorphic gradient is broadly perpendicular to the granite–greenstone contact and ranges from upper greenschist facies conditions in the structurally highest Fig Tree Group to upper amphibolite facies conditions in the Onverwacht Group. It includes significant structural and, thus, metamorphic breaks, the most significant of which is the Consort Bar, along which, Onverwacht Group rocks (c. 600–700°C and 6–8 kbar) are juxtaposed against the overlying Fig Tree Group (c. 520–600°C and 4–5 kbar). Because the Consort Bar is itself folded, the early D_1-related structural imbrication and associated telescoping of metamorphic isograds must predate regional D_2 folding (Fig. 2). The progressive increase in peak temperatures from c. 520°C in the Western Zone to c. 590°C in the Eastern Zone in Fig Tree Group rocks above the Consort Bar (Fig. 7a), however, does not necessarily require any additional structural duplication, as rocks exposed in the Western Zone are more than 1 km higher in the structural sequence than those of the Central and Eastern Zones. Different temperature conditions may thus be explained by the different structural positions in the mine. Assuming a constant geothermal gradient of c. 40°C/km within the Fig Tree Group, the inferred peak pressures in the Western Zone, for which no pressure estimates could be made, are at c. 4 kbar.

Figure 11 shows the peak metamorphic P–T conditions compared to the estimated temperature conditions during mineralization in the three areas investigated. The temperature estimates of 680±25°C for the early mineralization in the Eastern Zone are, within error, indistinguishable from temperatures estimated for the peak of metamorphism in the Onverwacht Group (Fig. 11b). This suggests that the early mineralization may correlate with the local D_1 deformation. The main stage of gold mineralization, however, correlates with the local D_2 deformation. The D_2 deformation is marked by the development of discrete ductile shear zones that crosscut the D_1 fabrics in the central parts of the mine as well as a reactivation of the earlier Consort Bar in sites of favorable orientation. The mineralized D_2 shear zones are commonly associated with the intrusion of c. 3,040 Ma syn- to post-kinematic pegmatite dykes that can locally be shown to truncate the regional folds (Figs. 2 and 4; Harris et al. 1995). In the Western and Central Zones, the temperatures of the main stage mineralization are similar to the peak metamorphic temperatures of the Fig Tree Group (Fig. 11a, Tables 4 and 7). In contrast, the footwall lens mineralization in Onverwacht Group rocks of the Eastern Zone occurred at

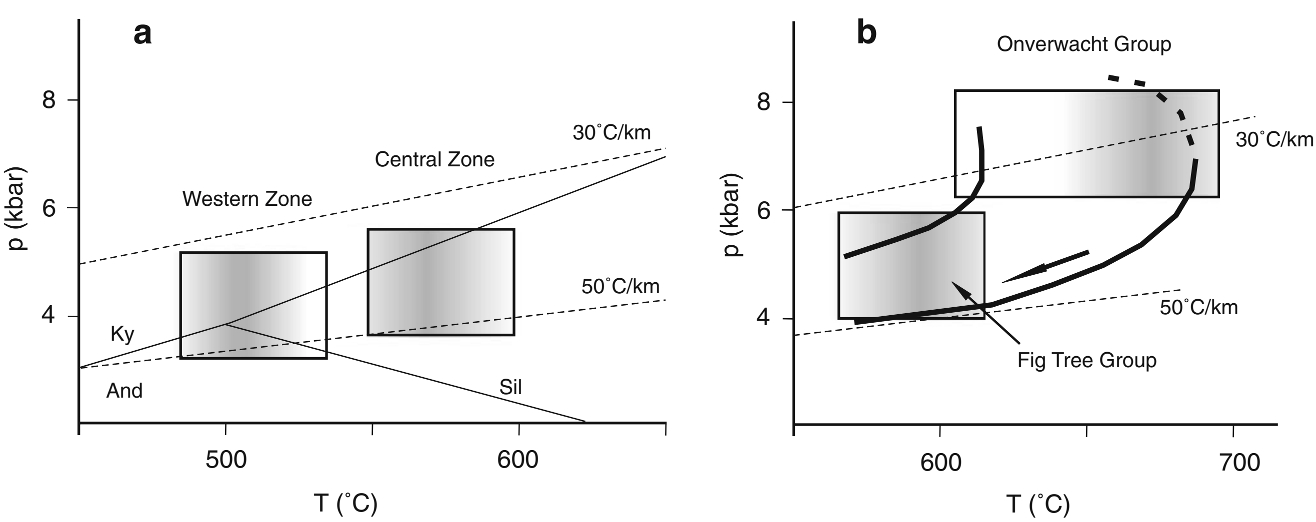

Fig. 11 P–T diagrams comparing the peak metamorphic conditions of host lithologies (*squares*) and temperature conditions of mineralization (*gray-shaded areas*) in **a** the Western and Central Zones and **b** the Eastern Zone. The *arrow* marks the retrograde P–T path of the footwall rocks

temperature conditions some 50–100°C lower than those of the peak of metamorphism (Fig. 11b). Importantly, the temperature conditions of this retrograde mineralization are also consistent with those estimated for the structurally overlying metapelites (Fig. 11b, Table 7). Thus, the main stage of gold mineralization in all three localities occurred at temperature conditions corresponding to the peak conditions of Fig Tree Group rocks in the hanging wall, while the Onverwacht Group rocks in the footwall of the Consort Bar were on their retrograde path. A contemporaneous timing for the main stage of gold mineralization in all zones throughout the New Consort Mine is also supported by the close spatial relationship of mineralized D_2 structures and syn-kinematic pegmatites dykes in the Central and Eastern Zones (Fig. 4). The estimated temperatures, as well as the distinct change of sulfide and alteration assemblages with increasing metamorphic grade, indicate that the temperature gradient recorded in rocks of the Fig Tree Group was present during the main stage gold mineralization, pointing to a causal relationship between the juxtaposition of footwall rocks with the Fig Tree Group and the gold mineralization.

While the absolute timing of the sequence of deformation and mineralization events remains unknown, the established relative timing relationships between the metamorphic evolution of the wall rocks and the gold mineralization have also important implications for the origin of the mineralizing fluids. Metamorphic devolatilization reactions within the greenstone belt seem unlikely to have been a source of the mineralizing fluids because the basal greenstone sequences, i.e., the upper amphibolite facies rocks in the footwall of the Consort Bar, were already on their retrograde path. Also, the largest volume of metamorphic fluids produced to form mineralizing hydrothermal systems results from dehydration reactions at conditions corresponding to the greenschist–amphibolite facies transition (e.g., Ridley et al. 2000), suggesting dehydration reactions at conditions identical to those estimated for the main stage of gold mineralization. An external fluid source is also consistent with the work by de Ronde et al. (1992) and Dziggel et al. (2006) who concluded that the peak of regional metamorphism correlates with the regional D_2 deformation at c. 3,230 Ma, and thus, predates the gold mineralization by more than 150 My. This suggests that the local D_2 deformation outlined above, as well as the peak of metamorphism in the Fig Tree Group, must be related to a later thermal event. Other potential mechanisms to create such large hydrothermal systems, such as magma crystallization at depth, appear to be in conflict with the available geochronological data, as the emplacement of the late potassic granites at c. 3,100 Ma predates the gold mineralization by at least 20 My (de Ronde et al. 1992). Also, the lower grade metamorphic overprint observed in the Fig Tree Group suggests a major second metamorphic event that was associated with considerably higher geothermal gradients. This event is not recorded in the Onverwacht Group, implying that these rocks had been dehydrated previously. We thus suggest a prograde dehydration of the crust below the greenstone belt during the late tectonic history of the greenstone belt as the most likely source for the gold-bearing fluids. This event must have had a major impact on the juxtaposition of footwall rocks against the Fig Tree Group, and thus, on the final architecture of the greenstone belt.

Acknowledgments The authors are grateful to the mine management of the Barberton Mines Ltd. for access to underground workings and drill core. R. Carey and R. le Roux are thanked for fruitful discussions in the field. A. Otto acknowledges financial support from the Society of Economic Geology (SEG) and the German Academic Exchange Service (DAAD). J. Kolb is thanked for reviewing an earlier version of the manuscript. Constructive reviews by H. Frimmel and B. Lehmann considerably improved the manuscript, and are greatly appreciated.

References

Andrews AJ, Hugon H, Durocher M, F, Lavigone MJ (1986) The anatomy of a gold-bearing greenstone belt: Red Lake, northwestern Ontario, Canada. In: Macdonald AJ (ed) Proceedings of Gold ’86, an International Symposium on the Geology of Gold Deposits, Toronto, pp 3–22

Anhaeusser CR (1972) The geology of the Jamestown Hills area of the Barberton Mountain Land, South Africa. In: Verhandelinge van die Geologiese Vereniging van Suid Afrika. Transactions of the Geological Society of South Africa 75:225–263

Anhaeusser CR (1986) Archean gold mineralization in the Barberton Mountain Land. In: Anhaeusser CR, Maske S (eds) Mineral deposits of Southern Africa, I. Geol Soc S Afr, pp 113–154

Anhaeusser CR, Viljoen MJ (1965) The base of the Swaziland system in the Barberton-Noordkaap-Louw’s Creek area, Barberton Mountain Land. In: Information Circular—University of the Witwatersrand, Economic Geology Research Unit, 25:32

Byerly GR, Kroner A, Lowe DR, Todt W, Walsh MM (1996) Prolonged magmatism and time constraints for sediment deposition in the early Archean Barberton greenstone belt: evidence from the Upper Onverwacht and Fig Tree Groups. Precambrian Res 78:125–138

Cloete M (1999) Aspects of volcanism and metamorphism of the Onverwacht Group lavas in the southwestern portion of the Barberton greenstone belt. Mem Geol Surv S Afr 84:232

de Ronde CEJ, de Wit MJ (1994) Tectonic history of the Barberton greenstone belt, South-Africa—490 million years of Archean crustal evolution. Tectonics 13:983–1005

de Ronde CEJ, Kamo SL (2000) An Archaean arc–arc collisional event: a short-lived (ca 3 Myr) episode, Weltevreden area, Barberton greenstone belt, South Africa. J Afr Earth Sci 30:219–248

de Ronde CEJ, Kamo S, Davis DW, Dewit MJ, Spooner ETC (1991) Field, geochemical and U–Pb isotopic constraints from hypabyssal felsic intrusions within the Barberton greenstone belt, South-Africa—implications for tectonics and the timing of gold mineralization. Precambrian Res 49(3–4):261–280

de Ronde CEJ, Spooner ETC, Dewit MJ, Bray CJ (1992) Shear zone-related, Au quartz vein deposits in the Barberton greenstone belt, South-Africa—field and petrographic characteristics, fluid properties, and light stable isotope geochemistry. Econ Geol 87:366–402

Diener JFA, Stevens G, Kisters AFM, Poujol M (2005) Metamorphism and exhumation of the basal parts of the Barberton greenstone belt, South Africa: Constraining the rates of Mesoarchaean tectonism. Precambrian Res 143:87–112

Dupré B, Arndt NT (1990) Pb isotopic compositions of Archean komatiites and sulfides. Chem Geol 85:35–56

Dziggel A, Stevens G, Poujol M, Anhaeusser CR, Armstrong RA (2002) Metamorphism of the granite–greenstone terrane south of the Barberton greenstone belt, South Africa: an insight into the tectono-thermal evolution of the 'lower' portions of the Onverwacht Group. Precambrian Res 114:221–247

Dziggel A, Knipfer S, Kisters AFM, Meyer FM (2006) P–T and structural evolution of high-T, medium-P basement rocks in the Barberton Mountain Land, South Africa. J Metamorph Geol 24: 535–551

Goldfarb RJ, Groves DI, Gardoll S (2001) Orogenic gold and geologic time: a global synthesis. Ore Geol Rev 18:1–75

Goldfarb RJ, Baker T, Dubé B, Groves DI, Hart CJR, Gosselin P (2005) Distribution, character, and genesis of gold Deposits in metamorphic terranes. Econ Geol 100th anniversary volume, 407–450

Groves DI (1993) The crustal continuum model for late-Archaean lode-gold deposits of the Yilgarn block, Western Australia. Miner Depos 28:366–374

Groves DI, Goldfarb RJ, Gebre-Mariam M, Hagemann S, Robert F (1998) Orogenic gold deposits: a proposed classification in the context of their crustal distribution and relationship to other gold deposit types. Ore Geol Rev 13:7–28

Groves DI, Goldfarb RJ, Knox-Robinson CM, Ojala J, Gardoll S, Yun GY, Holyland P (2000) Late-kinematic timing of orogenic gold deposits and significance for computer-based exploration techniques with emphasis on the Yilgarn block, Western Australia. Ore Geol Rev 17:1–38

Groves DI, Goldfarb RJ, Robert F, Hart CJR (2003) Gold deposits in metamorphic belts: overview of current understanding, outstanding problems, future research, and exploration significance. Econ Geol 98:1–29

Hagemann SG, Cassidy KF (2000) Archean orogenic lode gold deposits. In: Hagemann SG, Brown PE (eds) Gold in 2000: reviews in economic geology, vol 13, pp 9–68

Harris PD, Smith CB, Hart RJ, Robb LJ (1993) Sm–Nd and Rb–Sr isotope systematics of rare-element pegmatites from the New Consort Gold Mines, Barberton Mountain Land, South Africa. In: Information Circular—University of the Witwatersrand, Economic Geology Research Unit 265:20

Harris PD, Robb LJ, Tomkinson MJ (1995) The nature and structural setting of rare-element pegmatites along the northern flank of the Barberton greenstone belt, South Africa. S Afr J Geol 98:82–94

Holdaway MJ (2000) Application of new experimental and garnet Margules data to the garnet–biotite geothermometer. Am Mineral 85:881–892

Holland TJB, Blundy J (1994) Non-ideal interactions in calcic amphiboles and their bearing on amphibole-plagioclase thermometry. Contrib Mineral Petrol 116:433–447

Holland TJB, Powell R (1998) An internally consistent thermodynamic data set for phases of petrological interest. J Metamorph Geol 16:309–343

Kamo SL, Davis DW (1994) Reassessment of Archean crustal development in the Barberton Mountain Land, South-Africa, based on U–Pb dating. Tectonics 13:167–192

Kerrich R, Cassidy KF (1994) Temporal relationship of lode gold mineralization to accretion, magmatism, metamorphism and deformation—Archean to present: a review. Ore Geol Rev 9:263–310

Kisters AFM, Stevens G, Dziggel A, Armstrong RA (2003) Extensional detachment faulting at the base of the Barberton greenstone belt: evidence for a 3.2 Ga orogenic collapse. Precambrian Res 127:355–378

Kretz R (1983) Symbols for rock-forming minerals. Am Mineral 68(1–2):277–279

Krogh EJ (1988) The garnet-clinopyroxene Fe-Mg geothermometer—a reinterpretation of existing experimental-data. Contrib Mineral Petrol 99:44–48

Kröner A, Byerly GR, Lowe DR (1991) Chronology of early Archean granite–greenstone evolution in the Barberton Mountain Land, South-Africa, based on precise dating by single zircon evaporation. Earth Planet Sci Lett 103(1–4):41–54

Kröner A, Hegner E, Wendt JI, Byerly GR (1996) The oldest part of the Barberton granitoid–greenstone terrain, South Africa: evidence for crust formation between 3.5 and 3.7 Ga. Precambrian Res 78:105–124

Lahaye Y, Arndt N, Byerly, G, Chauvel C, Fourcade S, Gruau G (1995) The influence of alteration on the trace-element and Nd isotopic compositions of komatiites. Chem Geol 126(1):43–64

Lowe DR, Byerly GR (1999) Stratigraphy of the west-central part of the Barberton greenstone belt. In: Lowe DR, Byerly GR (eds) Geological evolution of the Barberton greenstone belt, 329. Special Paper of the Geological Society of America, South Africa, pp 1–36

McCuaig TC, Kerrich R (1998) P–T–t deformation fluid characteristics of lode-gold deposits: evidence from alteration systematics. Ore Geol Rev 12:381–453

McCuaig TC, Kerrich R, Groves DI, Archer N (1993) The nature and dimensions of regional and local gold-related hydrothermal alteration in tholeiitic metabasalts in the Norseman goldfields—the missing link in a crustal continuum of gold deposits. Miner Depos 28:420–435

Plyusnina LP (1982) Geothermometry and geobarometry of plagioclase–hornblende bearing assemblages. Contrib Mineral Petrol 80(2): 140–146

Ravna EK (2000a) Distribution of Fe2+ and Mg between coexisting garnet and hornblende in synthetic and natural systems: an empirical calibration of the garnet–hornblende Fe–Mg geothermometer. Lithos 53:265–277

Ravna EK (2000b) The garnet–clinopyroxene Fe2+–Mg geothermometer: an updated calibration. J Metamorph Geol 18:211–219

Ridley JR, Groves DI, Knight JT (2000) Gold deposits in amphibolite and granulite facies terranes of the Archean Yilgarn Craton, Western Australia: evidence and implications of synmetamorphic mineralization. Rev Econ Geol 11:265–290

Robertson MJ, Charlesworth EG, Phillips GN (1994) Gold mineralization during progressive deformation at the Main Reef Complex, Sheba Gold Mine, Barberton greenstone belt, South-Africa. Explor Min Geol 3:181–194

Schouwstra RP (1995) Wall-rock alteration as a guide to gold-bearing fracture zones in the Zwartloppie section, Sheba Gold Mine, South Africa. S Afr J Geol 98:399–414

Schouwstra RP, deVilliers JPR (1988) Gold mineralization and associated wallrock alteration in Main Reef Complex at Sheba Mine, South Africa. Trans Inst Min Metall B Appl Earth Sci 97: B158–B170

Schürmann LW, Ward JHW, Horstmann UE, Jordaan LJ, Eaton B (2000) Carbonate dykes associated with Archaean lode–Au mineralization, Barberton greenstone belt, South Africa. J Afr Earth Sci 30:249–266

Sengupta P, Dasgupta S, Bhattacharya PK, Hariya Y (1989) Mixing behavior in quarternary garnet solid-solution and an extended Ellis and Green garnet-clinopyroxene geothermometer. Contrib Mineral Petrol 103:223–227

Sharp ZD, Essene EJ, Kelly WC (1985) A reexamination of the arsenopyrite geothermometer—pressure considerations and applications to natural assemblages. Can Mineral 23:517–534

South African Committee for Stratigraphy (SACS) (1980) Stratigraphy of South Africa. Part 1: lithostratigraphy of the Republic of Africa, South West Africa/Namibia, and the Republics of Bophuthatswana, Transkei and Venda. Handbook of the Geological Survey of South Africa 8:690

Spear FS (1993) Metamorphic phase equilibria and pressure–temperature–time paths. Mineralogical Society of America Monograph, Washington, DC, p 799

Tegtmeyer AR, Kröner A (1987) U–Pb zircon ages bearing on the nature of early Archean greenstone-belt evolution, Barberton Mountainland, Southern-Africa. Precambrian Res 36(1):1–20

Tomkinson MJ, Lombard A (1990) Structure, metamorphism, and mineralization in the New Consort Gold Mines, Barberton greenstone belt, South Africa. In: Glover JE, Ho SE (eds) Third International Archean Symposium, Perth, 1990. Ext. Abstrs. Volume, Geoconferences (WA) Inc., Perth, pp 377–379

Voges FD (1986) The New Consort Gold Mine, Barberton greenstone belt. In: Anhaeusser CR, Maske S (eds) Mineral deposits of Southern Africa, I&II. Geological Society of South Africa, pp 163–168

Witt WK, Vanderhor F (1998) Diversity within a unified model for Archaean gold mineralization in the Yilgarn Craton of Western Australia: an overview of the late-orogenic, structurally-controlled gold deposits. Ore Geol Rev 13:29–64

Wu CM, Zhang J, Ren LD (2004) Empirical garnet–biotite–plagioclase–quartz (GBPQ) geobarometry in medium- to high-grade metapelites. J Petrol 45:1907–1921